Nanoscale Advances

ROYAL SOCIETY OF CHEMISTRY

REVIEW

View Article Online
View Journal | View Issue

Cite this: *Nanoscale Adv.*, 2020, **2**, 3734

Role of inorganic nanoparticle degradation in cancer therapy

Christy Maksoudian, Neshat Saffarzadeh, Evelien Hesemans, Nora Dekoning, Kiana Buttiens and Stefaan J. Soenen *

Nanomaterials are currently widely exploited for their potential in the development of novel cancer therapies, and so far, mainly nanoparticles (NPs) consisting of liposomes and polymers have made their way into the clinic. However, major bottlenecks for the clinical translation of other types of NPs (*i.e.* inorganic) are the lack of knowledge concerning their long-term distribution *in vivo* and their potential toxicity. To counter this, various research groups have worked on soluble NPs, such as zinc oxide (ZnO), copper oxide (CuO), and silver (Ag), which tend to dissolve spontaneously into their ionic form, releasing toxic metal ions and leading to reactive oxygen species (ROS) generation when exposed to cellular environments. By fine-tuning the dissolution kinetics of these NPs, it is possible to control the level of ROS production and thus cytotoxicity to selectively destroy tumor tissue. Specifically, cancer cells tend to exhibit a higher basal level of oxidative stress compared to normal cells due to their higher metabolic rates, and therefore, by engineering NPs that generate sufficient ROS that barely exceed toxic thresholds in cancer cells, normal cells will only experience reversible transient damage. This review focuses on the use of these soluble inorganic NPs for selective cancer therapy and on the various *in vitro* and *in vivo* studies that have aimed to control the dissolution kinetics of these NPs, either through particle doping or surface modifications.

Received 10th April 2020
Accepted 25th July 2020

DOI: 10.1039/d0na00286k

rsc.li/nanoscale-advances

1. Introduction

Despite the long use of nanomaterials for biomedical applications, the field of nanomedicine only truly established itself as a separate field from nanotechnology in 2004 and involves the use of nanoparticles (NPs) that range from one to hundreds of nanometers for medical purposes.[1] At this small scale, the surface area is significantly increased, altering the physical and chemical characteristics of the particles and giving rise to their various unique properties that render them suitable for a wide range of biomedical applications.[2–4] For instance, NPs with varying compositions, sizes, and shapes can be used to enhance the solubility, biodistribution, and magnetic and optical properties of formulations, while their surfaces can be

Department of Imaging and Pathology, KU Leuven, NanoHealth and Optical Imaging Group, Herestraat 49, B3000, Belgium. E-mail: s.soenen@kuleuven.be; Tel: +32 16 330034

Christy Maksoudian obtained her BSc in Biomedical Sciences from New York University and MSc in Drug Discovery and Development from Imperial College London, during which she worked extensively on the use of cell-penetrating peptides and gold nanoparticles in cancer therapy, respectively. She is currently pursuing her PhD at KU Leuven, with her work mainly focusing on the optimization of nanoparticle delivery to solid tumors using a variety of biological methods, particularly cell-based therapy.

Neshat Saffarzadeh obtained her Masters' degree in Microbial Biotechnology from the University of Tehran in Iran in 2017 and is currently pursuing her PhD in Biomedical Science at KU Leuven under the supervision of Prof. Stefaan Soenen. Her research involves the use of various doped metal oxide nanoparticles for the treatment of cancer as well as bacterial and fungal infections.

functionalized with various coatings and ligands to improve tissue selectivity and uptake into targeted cells.[5,6] A wide range of different materials including liposomes, polymers, micelles, metal oxides (MOs) and other inorganic components can be employed for NP synthesis. These NPs can be subdivided in several ways based on their various characteristics. Two classifications that are often employed include chemical composition (organic or inorganic) and use (as delivery vehicle or direct physical/chemical therapy).

The focus of nanomedicine in the clinic so far has been in the treatment of cancer (*i.e.* Doxil©, Abraxane©, Onivyde MM-398©, DaunoXome©), anemia and Fe deficiency (*i.e.* Cosmofer©, Feraheme©), and infections (*i.e.* AmbiSome©), and in their use as contrast agents for non-invasive imaging (*i.e.* Ferumoxtran-10©, SonoVue©) and in vaccinations (*i.e.* Epaxal©, Inflexal©). Specifically, the anticancer regimens Doxil© and DaunoXome© consist of liposomes loaded with doxorubicin (DOX) and daunorubicin, respectively, and are approved for the treatment of HIV-associated Kaposi's sarcoma. Additional indications for Doxil© include ovarian cancer and multiple myeloma. Moreover, the approval of no less than three new nanomedicines, VYXEOS© (FDA-approved), Patisiran© (FDA-approved) and Hensify© (CE-Mark approved), in the last couple of years clearly shows that the field of nanomedicine is being actively investigated in by companies and academic and research institutions worldwide.[7] VYXEOS© consists of liposomes loaded with daunorubicin and cytarabine and was approved for the treatment of acute myeloid leukemia cancer in 2017. Hensify©, on the other hand, is a hafnium oxide NP-based aqueous suspension that is used for enhanced radiotherapy treatment and was recently approved in 2019. Patisiran©, the first siRNA/RNAi therapeutic, is also encapsulated within liposomes and has received FDA-approval in 2018 for the treatment of rare amyloidogenic polyneuropathy. Currently, there are a few thousand ongoing studies that use NPs mainly focusing on cancer and gene therapy.[7] These studies mostly involve the so-called 'soft' NPs, consisting of liposomes or polymers, which predominantly aim to obtain a more efficient delivery of traditional anticancer agents (Fig. 1).

Harder NPs, often consisting of inorganic metals or MOs, have lower translational use, although a lot of progress has been made over the last years. For example, Fe oxide (IO) NPs

Evelien Hesemans obtained a Masters' degree in Pharmaceutical Sciences in 2017, with a specialization in Drug Development, followed by a Master in Management, both at KU Leuven. At the moment she is a PhD candidate in the Nano-Health and Optical Imaging lab supervised by Prof. Soenen. Her PhD project focuses on the development and validation of optical imaging tools for advanced preclinical cancer research. She strives to design an imaging platform to visualize small cell numbers including therapy-resistant cells, cells undergoing EMT and cancer stem cells.

Kiana Buttiens is a PhD candidate in the Doctoral School of Biomedical Sciences, within the domain of Cancer. After receiving her Masters' degree in Biochemistry and Biotechnology from KU Leuven in 2018, she joined Prof. Soenen's Nano-Health and Optical Imaging Lab. Her research focuses on the use of nanoparticles in cancer therapy, mainly exploring their effect on extracellular vesicle-mediated cellular communication.

Nora Dekoning graduated from the University of Antwerp with a Master's degree in Biochemical Engineering Technology in 2018. She joined the lab of Prof. Soenen at KU Leuven in 2019 as a PhD student in Biomedical Sciences in the cancer doctoral school. The main focus of her PhD is developing biomimetic nanoparticles for the optimization of innovative optical imaging techniques.

Stefaan J. Soenen heads the NanoHealth and Optical Imaging Group at KU Leuven, Belgium since January 2018. His main research interests lie in the use of nanomaterials for therapeutic and diagnostic purposes and on developing novel preclinical optical imaging methods. He has published over 75 manuscript with an h-index of 34 and received an ERC Starting Grant for his work on nanotherapeutics for cancer therapy.

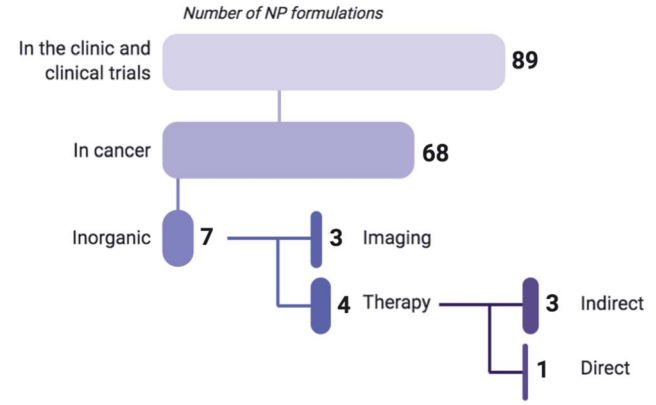

Fig. 1 Based on a recent review by Anselmo and Mitragotri (2019) listing 89 NP formulations that are currently approved for use in the clinic or undergoing clinical trials, 75% of these regimens are indicated for cancer treatment (including gene therapy) or diagnosis, of which 90% are composed of organic materials such as liposomes, polymers and micelles.[7] Six of the inorganic NP formulations that are clinically approved are used for imaging, while only one (NU-0129) functions as a direct therapeutic. As of 2019, NU-0129, consisting of Au NPs surface-covered with nucleic acids, is being tested in phase I clinical trials for the treatment of glioblastoma. The indirect-acting NPs exert their anticancer activity through radiation or thermal ablation by an external source.

are already clinically approved as hyperthermia agents for the treatment of multiforme glioblastoma (MagForce©) and are currently being tested on other types of tumors such as prostate cancer. Gold (Au) NPs are also being investigated in diverse cancer studies as agents for photothermal therapy (Aurolase©). In both cases, the NPs are used as indirect therapeutic agents, where external stimuli such as alternating magnetic fields and laser lights are applied upon administration of MagForce© and Aurolase©, respectively, to produce local heat, leading to cancer cell (CC) death. The lower translation of such NPs in the clinic has mainly been attributed to the lack of knowledge concerning their safety due to their potential to induce high levels of toxicity in biological systems compared to their bulk counterparts.[8] This can be explained by the greater number of reactive sites on the NP surface associated with their higher surface-to-volume ratio as well as the high chemical reactivity that results from the structural modifications of their surface electronic properties.[9,10] Concurrently, their nano size enables them to circumvent clearance by the reticuloendothelial system (RES), remain longer in blood circulation,[11] passively traverse across the leaky tumor vasculature and penetrate deep into tumor tissue – a phenomenon known as the enhanced permeability and retention (EPR) effect.[12,13] Put together, the larger exposure of the surface reactivity of NPs and their EPR effect lead to a higher level of particle interaction with their immediate surroundings, and therefore, greater potential for toxicity. However, this may not be the case for all types of materials, and even within a single type, the degree of toxicity is dependent upon multiple factors such as size, shape, coating and other surface modifications, as well as the nature of the exposed cell type.[6,14–16]

Therefore, there is a strong need to control NP-induced toxicity for effective tumor therapy. Alongside unaccounted-for toxicity, another factor that restricts the use of NPs in the clinic is the limited knowledge concerning their final destination, especially in the long-term. For example, Au NPs remain in the body for a long time and it is not yet entirely clear where these NPs will go after the therapy has been completed and what their long-term effects are, mainly in terms of the immune system, liver, spleen and kidneys.[17–19] It has been suggested that such NPs remain intact within the tumor environment as a result of the thick extracellular matrix, poor lymphatic drainage, and eventual particle agglomeration. To counter this, various research groups have worked on soluble NPs, such as zinc oxide (ZnO), copper oxide (CuO), and silver (Ag). These NPs tend to dissolve spontaneously into their ionic form, releasing toxic metal ions (M^{z+}) when exposed to biotic/abiotic environments.[20,21] In the context of the cell, the NPs are mainly taken up by endocytosis, during which their M^{z+} release induces reactive oxygen species (ROS)-mediated toxicity in tumor tissues. This review will discuss the mechanisms by which these inorganic NPs degrade and exert their cytotoxicity, and how controlling the degree of M^{z+} release from NPs can be harnessed to achieve selective tumor therapy. Although IONPs are the one of the most commonly used type of inorganic NPs for biomedical applications to date, their intracellular degradation has thus far not been linked to a cancer-selective toxicity (to our knowledge) particularly since the release of ferric ions is easily incorporated into the natural metabolism of the cell to be used in various biological functions and is thus tolerated at high levels.[22] Therefore, this review will mainly focus on ZnO, CuO, and Ag NPs.

2. Inorganic NPs and their degradation

For all engineered NPs to be used for biomedical applications, their potential toxicity and removal from the body must be studied. In general, for organic materials, most commonly applied materials are biodegradable, resulting in the generation of biologically relevant components (*e.g.* polylactic-*co*-glycolic acid (PLGA) breaks down into lactic and glycolic acid, which are metabolites that can be processed in cellular Krebs cycle[23]). While the effect of these additional metabolites on cell growth and metabolism may not be negligible in all conditions, the toxicity thereof will be minimal. For inorganic NPs, this is typically a far more difficult story. Some NPs, such as Au NPs tend not to degrade and can persist very long inside the body.[17] Other NPs can degrade, upon which they release M^{z+}. Any toxicity associated with this depends on multiple factors, including the chemical nature of the ions released and the rate of degradation. It is important to note that while some ions are physiologically relevant (*e.g.* Zn, Fe), their presence may affect other metabolites or disturb cellular homeostasis and hereby cause secondary toxicity. In the sections below, we aim to provide an overview of NP degradation (also referred to as "dissolution" throughout the text) with respect to how this can

affect cellular homeostasis and how the process of NP degradation can be more controlled to selectively destroy CCs. Specifically, given that CCs exhibit a higher basal level of ROS compared to normal cells (NCs) due to their higher metabolic rates, NPs can be engineered to release M^{z+} and generate ROS at finely-tuned levels that exceed toxic thresholds in CCs but only cause transient cellular damage in healthy tissue and allow gradual recovery.

2.1. Oxidative stress due to M^{z+} release from inorganic NPs as main cause of toxicity

The mechanism by which metallic NPs exert their cytotoxic effects has been mainly attributed to the generation of ROS or ROS-induced damage (Fig. 2).[4,24] These species can be classified as non-radicals (*i.e.* H_2O_2, HOCl, O_3) or free radical-containing (*i.e.* $^1O_2$, $O_2^{\bullet -}$, $HO^{\bullet}$, $HO_2^{\bullet}$).[25,26] Under normal conditions, ROS are produced as intermediates by the cell's natural oxidative metabolism and serve as key mediators in processes such as cell survival and signaling, and production of inflammatory factors.[27,28] Their intracellular levels are strongly maintained by antioxidants (*i.e.* glutathione GSH), and detoxifying enzymes, including superoxide dismutases (SODs), GSH peroxidase (GPx), and catalase (CAT).[29] SOD serves as a catalyst for the conversion of O_2^- to O_2 and H_2O_2, and CAT further reduces H_2O_2 to H_2O. The cellular compartments that are mainly associated with ROS production are the mitochondria, endoplasmic reticula (ER), peroxisomes, and NADPH oxidase (NOX) complexes located on the cell membranes.[29–31] At the early stages of the ROS production process, increased levels of cytoplasmic calcium (Ca^{2+}) trigger the activation of the mitochondrial electron transport chain, leading to the production of ATP and therefore, ROS as by-products.[32,33] Disruption in the redox balance that regulates ROS homeostasis leads to the oxidative damage of various biomolecules and consequently, interference with different cellular functions.[34,35] Among the alterations that ROS generation exert is the peroxidation of lipids leading to cell membrane damage, oxidation of proteins which interferes with enzymatic function and membrane permeability, and nucleic acid oxidation that causes genotoxicity.[4,36] ROS-induced oxidative stress has been delineated as a three-tier model.[35,37] Tier 1 is characterized by a defensive response wherein detoxifying enzymes including HO1, NAD(P)H, SOD and CAT aim to restore the redox balance and minimize damage through the activation of the phase II genes by Nrf2.[38,39] Tier 2 results from ROS-induced stress that surpasses the enzymes' defensive capacity, leading to the production of pro-inflammatory cytokines and chemokines and thus, activation of inflammatory cells such as macrophages and neutrophils.[40,41] Among the pro-inflammatory responses is the activation of mitogen-activated protein kinase (MAPK) and nuclear factor κB (NFκB).[42,43] Tier 3 involves

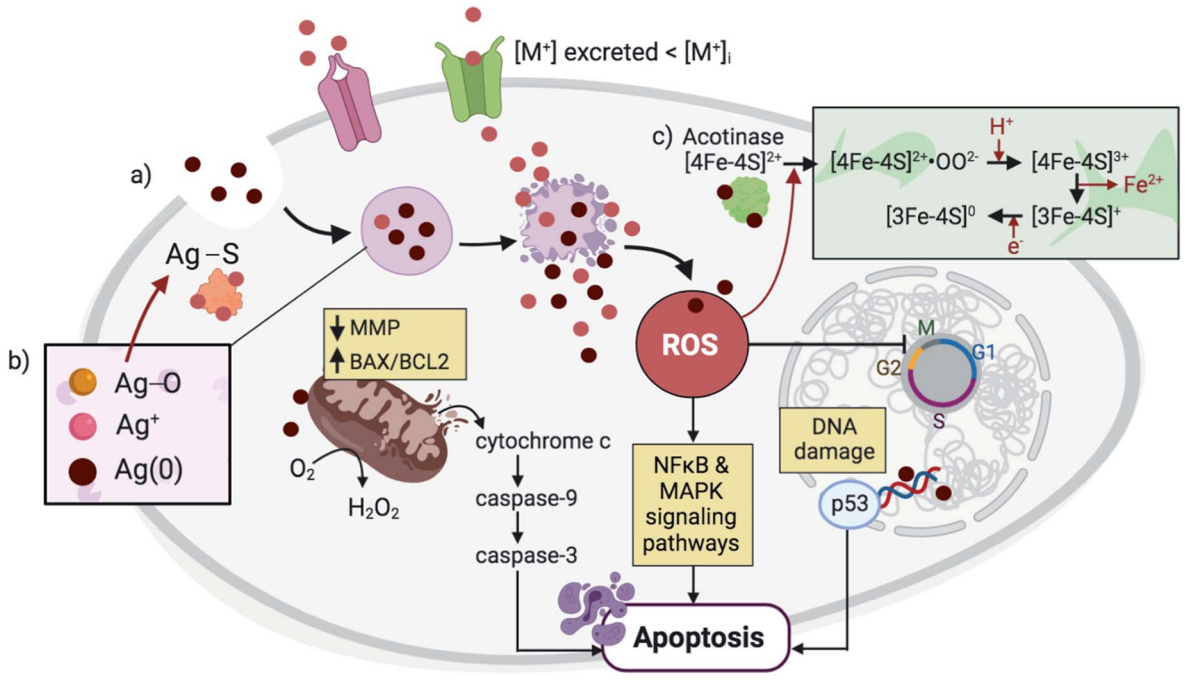

Fig. 2 NPs are endocytosed and are contained within lysosomal compartments, during which they are exposed to low pH environments that accelerate their dissolution. (a) The high concentration of local M^{z+} release (pink) exceeds the metal transporters' capacity to excrete ions, leading to ROS generation and DNA damage. In response, *p53* triggers cell cycle arrest with the aim of restoring oxidative balance. Further elevation in ROS levels causes a decrease in the MMP and an increase in the BAX/BCL2 ratio, triggering cytochrome c release and activation of a caspase signaling pathway that leads to apoptosis. Other signaling pathways such as NFκB and MAPK are also activated during NP-mediated apoptosis. (b) In the case of Ag NPs, three forms of Ag exist simultaneously in the lysosomes, including solid Ag(0), Ag^+, and Ag_2O.[65] Subsequent interaction of Ag_2O intermediates with cysteine residues results in Ag–S formation that cause disruptions in protein secondary structures. (c) Meanwhile, in the case of ZnO NPs, M^{z+} release and ROS generation cause alterations in the Fe–S clusters that are found abundantly in several protein families including aconitase, leading to protein inactivation.[42]

perturbation of the mitochondrial membranes and their potential through the formation of transient pores and increased influx of intracellular calcium, resulting in morphological changes or cell death by apoptosis, autophagy or necrosis.[35] When NPs are internalized by the cells, they are taken up into the endosomes where the acidic environment and cellular biomolecules stimulate metal ion release from the NPs causing an imbalance in the local metal ion homeostasis and producing a strong but gradual increase in ROS that reaches optimum/Tier 3 levels after 24–48 h. Specifically, transition metals located at the surface of NPs, such as Cu on CuO NPs, have been shown to react with H_2O_2 to produce $HO^{\bullet}$ and oxidized Cu ions *via* Fenton-type reactions.[44,45]

2.1.1. M^{z+} released from NPs *vs.* their metal salt counterparts. It is generally agreed upon that the toxicity induced by these dissolving inorganic NPs is at least partially due to the release of M^{z+}.[20] Several studies have been conducted throughout the years to confirm this hypothesis by comparing the toxicity induced by the NPs and their respective metal salts.[46–50] The "Trojan Horse" mechanism has been used to describe NP-associated cytotoxicity, which is predominantly mediated by particle uptake into lysosomes, followed by a burst-like release of Cu^{2+}, whereas the metal salts are not similarly internalized.[50,51] However, others have argued that ZnO and CuO NPs exert the same toxic effects as their ionic counterparts.[52–54] This strong discrepancy in the literature is a product of the different methodologies used in determining NP dissolution, as confirmed by Turney *et al.* (2012) revealing a fivefold difference in ZnO NP dissolution depending on whether the Zn species were separated by centrifugation or membrane filtration.[55] As a means to settle this debate, Ivask *et al.* (2017) used synchrotron radiation-based X-ray absorption near edge structure (SR-XANES) spectroscopy which does not require particle and ion separation to identify elemental speciation, and the resulting spectra delineated similar speciation profiles between ZnO and CuO NPs and their metal salts in cells and cell culture media.[56] Some have suggested that the observed toxicity within 24 h of NP exposure to cells is attributed to the NPs and their dissolution within the endosomes, while any subsequent effect is due to the M^{z+} that have diffused into the cytoplasm.[57,58] Concurrently, a bacterial proteomic study by Neal *et al.* (2012) has shown that in *Cupriavidus necator* bacteria, the proteins over-expressed upon ZnO NPs and Zn^{2+} exposure were associated with the synthesis of membrane proteins and cellular metabolism, respectively, suggesting varying mechanisms of toxicity induction of MO NPs and their salts.[59] Similarly, although higher cytotoxicity was detected for CuO NPs than $CuCl_2$, certain gene expression changes (*i.e.* for metallothioneins (MTs), which are key biomarkers in metal-induced toxicity[60]) were attributed to Cu^{2+} release.[46] However, it is now clear that NPs exhibit differing exposure kinetics than their respective metal salts. When cells are exposed to metal salts, the M^{z+} will typically diffuse throughout the entire cell almost uniformly. Conversely, once taken up by endosomes/lysosomes where the acidic environment speeds up their degradation (as will be explained more thoroughly in Section 2.2.1), NPs will locally induce high levels of M^{z+} within the vicinity or inside the endosomal compartments, which is quite different than what is observed in the rest of the cell. These high M^{z+} concentrations can locally exceed toxic thresholds while the overall cellular level may not be toxic. Combined with the oxidative stress linked to having the M^{z+} in the acidic environments of the endosomal compartment, this can give rise to higher levels of toxicity than free M^{z+} given in their salt form ref. 61.

As with CuO and ZnO NPs, there have been several debates on the cytotoxicity induced by Ag NPs and their metal salts. In a study by Kim *et al.* (2009), the authors demonstrate comparable levels of cytotoxicity between Ag NPs and $AgNO_3$, although the mechanism of toxicity differed for both.[62] In cells treated with Ag NPs, no particular effect on the expression of MTs could be detected, which contrasts with the increased expression observed in $AgNO_3$-exposed cells. When coupled with studies reporting that Ag NPs only partially dissolve in solution and thus release less free Ag^+ compared with Ag salt, these findings suggest that the Ag NPs-induced toxicity is a product of oxidative stress rather than M^{z+} release.[63] Given that the mechanism of Ag^+ release is shown to be *via* oxidative solution – during which surface metallic Ag reacts with protons and dissolved O_2 to yield Ag_2O, which is subsequently fully solubilized into Ag^+ – the partial dissolution of Ag NPs has been attributed to the Ag^+ readsorption onto the NP surface.[64,65] In fact, Liu and Hurt (2010) demonstrate that three forms of Ag are found in colloidal suspensions of Ag NPs, including solid Ag(0), Ag^+ that are available or have formed complexes with nutrients in the surrounding medium, and surface-adsorbed Ag^+.[65] The buildup of surface Ag^+, in turn, blocks the O_2 and proton access to metallic Ag, and this effect has been stated to be due to various NP surface coatings or particle agglomerations.[65,66] However, others have reported the full dissolution of Ag NPs, and theoretical calculations suggest that Ag NPs are fully soluble in solutions with pH ranging from 4 to 12.[65] At the same time, various studies have revealed that Ag NPs exhibit higher toxicity than Ag^+.[67,68] Specifically, a study by Eom and Choi (2010) indicates a time-dependent cytotoxic effect of Ag NPs,[69] an observation that is similar to one made by Llop *et al.* (2014) on ZnO NPs.[57] They show that, within 24 h of cellular incubation with Ag NPs and Ag^+, the levels of oxidative stress were similar for both species. After 24 h, Ag NPs exhibit significantly higher toxicity compared to free Ag^+, suggesting that they may serve as a long-term source of constant ion release. This data supports the notion that free M^{z+} disperse themselves throughout the cells, while NPs tend to accumulate within endosomal compartments and release their M^{z+} locally at high concentrations, exceeding toxic thresholds.

2.1.2. NP degradation disrupts the local M^{z+} homeostasis. Under normal physiological conditions, the lowly abundant free intracellular Zn^{2+} are mainly protein-bound (*i.e.* with MTs) or contained within lysosomes and mitochondria, and their homeostasis is maintained by the Zn transporters (ZnTs) and Zrt/Irt-like proteins (ZIPs) that decrease or increase the level of cytosolic Zn, respectively, through extracellular release or sequestration into organelles and vesicles.[70,71] In fact, ions of Zn and Cu that are located within the mitochondrial intermembrane space have been reported as catalysts in the conversion of

superoxide anions into H_2O_2.[72] Various ZnTs have been seen to co-localize with lysosomal proteins, and the increase in Zn^{2+} flux within lysosomes as a result of ZnT 2 overexpression highlights the importance of this organelle in maintaining cellular Zn levels.[71] Upon ZnO NP dissolution within the cells, the excess burst-like release of Zn^{2+} is much higher than the rate of ion excretion by ZnTs, which disturbs the local Zn homeostasis, leading to ROS generation. The Zn^{2+} tend to also accumulate within the mitochondria, causing the organelle's damage and loss of its membrane potential (MMP) and ultimately, apoptosis.[73] Among the various biological effects, Zn^{2+} have been shown to interfere with cytochrome bc1 and α-ketoglutarate dehydrogenase in complex III and I of mitochondria, respectively, significantly impeding the process of cellular respiration and leading to ATP depletion.[74–76] Furthermore, it has been reported that Zn^{2+} levels and their buffering capacity are generally lower in CCs – which have lower thresholds of oxidative stress compared to their normal counterparts.[77] As a result, the CCs tend to be more sensitive to elevating intracellular Zn^{2+} levels, providing a therapeutic window for ZnO NPs with finely-tuned dissolution kinetics to specifically target CCs.

Similarly, the homeostasis of Cu^{2+} is maintained by Cu importers such as CTR1 and ATPase that respectively increase or decrease the flux of Cu^{2+} within the cell.[78,79] When the level of intracellular Cu^{2+} is increased beyond normal conditions, CTR1 is internalized while ATPase is transferred to the cell membrane to eliminate the excess ions. However, during cellular uptake and subsequent dissolution of CuO NPs, the release of Cu^{2+} is significantly higher and more rapid than the capacity of ATPase to excrete the excess ions, disrupting the redox balance and inducing ROS generation and oxidative stress. The cellular homeostasis of Ag is also tightly regulated by metal transport genes and proteins. In a study by Wang *et al.* (2015), exposure of cells to Ag NPs led to an increase in mRNA expression levels of genes responsible for the extracellular release or sequestration of M^{2+} and metal-bound complexes into lysosomes, including ATP-binding cassette transporter subfamily C member C1 (ABCC1), divalent metal transporter 1 (DMT1) and Cu-transporting ATPase 1 (ATP7A).[80] The presence of Ag NPs within the lysosomal compartments also led to the disruption of the organelle membrane, followed by a significant reduction in MMPs after 24 h.

2.1.3. NP-induced DNA damage, autophagy, and necrosis. Elevated levels of oxidative stress may result in DNA damage (characterized by the phosphorylation of histone γ-H2AX[81]), which in turn stimulates the tumor suppressor gene *p53* to trigger cell cycle arrest as an attempt to reverse the damage or undergo self-apoptosis.[82,83] Whether a cell proceeds with apoptosis is determined by the ratio of pro-apoptotic BAX and anti-apoptotic BCL2 proteins.[84] Elevated BAX levels elicit the mitochondrial permeability transition and induce cytochrome c release from the mitochondrial outer membrane.[85,86] Once this process is triggered, DNA is fragmented at the internucleosomal linker sites and activated caspase-3 leads to autocatalysis and triggers a caspase signaling cascade.[87,88] Accordingly, exposure of different cell types to either ZnO, CuO or Ag NPs leads to overexpression of *p53*, *bax* and *caspase-3* and downregulation of *bcl2*.[89–91] Concurrently, the activities of SOD, CAT, and glutathione reductase (GSR) and GPx are significantly hindered as a result of NP treatment. While GSR recycles GSH disulfide to GSH and GPx converts lipid hydroperoxides to their hydroxyl form, they both contribute to the resistance towards oxidative stress. As such, due to the resulting NP-mediated antioxidant enzyme depletion, levels of intracellular ROS generation and lipid peroxidation become elevated, alongside intracellular Ca^{2+} flux, perturbation of mitochondrial membrane electron transfer and cell membrane leakage.[92] In attempt to reduce the oxidative damage incurred by NP-mediated ROS generation, exposed cells often undergo autophagy in response to mitochondrial damage, a process whereby the components of a cell such as its organelles are degraded and recycled and that eventually leads to cell death if progressed without interference.[93–95] Macroautophagy is the most commonly studied subtype of autophagy and involves the engulfment of the dysfunctional components by LC3-containing autophagosomes, followed by their delivery to the lysosomes, where local enzymes and the acidic pH initiate the degradation process. Among the accompanying cellular responses is the activation of the PI3K/AKT/mTOR signaling pathway. Another form of cell death that has been observed in MO NP-treated cells is necrosis, which is triggered secondarily in cases where apoptosis-associated caspase activation, cytochrome c release, and DNA fragmentation are hindered.[94,96,97] Molecules that have shown to be involved the initiation and modulation of necrosis include receptor-interacting proteins 1 (RIP1) and 3 (RIP3), caspase inhibitors, and poly(ADP-ribose) polymerase (PARP).[98] Although there is a general agreement regarding the cytotoxic effects of MO NPs, reported results still tend to vary among different studies due to inconsistencies in choices of assays, media, and other biological-related setups as well as differences in synthesis methods, which lead to varying structural defects and NP band structures.[99] Specifically, the positions of the valence and conduction band edges of a NP determine its band gap energy, which, in turn, dictates the level of electrons in the conduction band or electropositive holes in the valence band under varying conditions. In the intracellular setting, oxygen molecules can react with the conduction band electrons and valence band holes to produce $O_2^{\bullet-}$ (a precursor for the ROS $^{\bullet}OH$ and $^1O_2$) and $^{\bullet}OH$, respectively.[100]

2.2. Factors influencing NP dissolution

2.2.1. Effect of biological pH on NP dissolution. A major factor that impacts the solubility of these metal and MO NPs is the acidity in the surrounding medium.[101] These NPs have been shown to be significantly pH sensitive, with their dissolution proceeding much faster in acidic environments.[42,64] Specifically, ZnO NPs have shown to exhibit significantly high dissolution rates in low pH solutions (pH 1.5), reaching apparent equilibrium within 30 minutes, as compared with the equilibrium achieved after 60 minutes at neutral pH.[102] In a separate study, ZnO NPs dissolved fully at pH 6.1 and around 80% at pH 7.6 after 5 days in aqueous media.[101] Similar results have been confirmed for CuO NPs, in which ion measurements after 72 h of NP exposure in non-complexing buffer solutions indicate full

particle dissolution at pH 5.5.[103] Studies comparing Ag NP dissolution in neutral and acidic conditions have also revealed greater ion release at low pH.[65,104,105] Peretyazhko *et al.* (2014) explain that the possible mechanism behind this observation is that while the intermediate Ag_2O is covered with hydroxyl groups in water, its protonation under acidic conditions weakens the Ag–O bonds.[64] Given that NPs are typically taken up into the cells *via* endocytosis, they experience varying levels of acidity, from pH 7.4 in the extracellular environment to pH 5.5 within endosomes and pH 4.5 in lysosomes,[106] thereby releasing M^{z+} following acid etching upon exposure to endosomal compartments. The greater dissolution of NPs within lysosomes is also due to the high ionic strength and multitudes of hydrolytic enzymes, including cathepsin L, that non-specifically degrade the protein corona that is tightly bound to the particle surface as well as any polymer coating.[107–109] In fact, Kreyling *et al.* (2015) were able to reveal the clear separation between radiolabeled Au NPs and their radiolabeled polymer coat after being internalized within lysosomes.[110] More importantly, this highly pH-dependent dissolution kinetics can be exploited for further selective tumor therapy as the local pH in the tumor microenvironment is lower than in healthy tissue, triggering M^{z+} release preferentially in the vicinity of CCs.

2.2.2. Cellular proteins and amino acids affect NP dissolution. NP dissolution is also enhanced in nutrient-rich environments.[111] In cells, covalent complexation between the M^{z+} released from the MO NPs can occur with proteins or amino acids, causing crystal precipitation in the cytoplasmic fluid and ROS generation, which in turn can cause DNA damage and cell death following the Tier 3 biological pathways. In a recent work from our group, we show that Cu^{2+} released from CuO dissolution tend to complex with various amino acids and form light blue precipitates in glutamine solutions in the ratio 1 : 2, as confirmed using single-crystal X-ray diffraction (SC-XRD).[79] These findings are in line with previously reported structural formations between Cu^{2+} and glutamine.[112] In fact, several early works have described the crystal structure that results from Cu^{2+} complexation with various amino acids, such as asparagine,[113] glutamic acid[114] and aspartic acid.[115] Records of electron paramagnetic resonance (EPR) spectra in growth medium also indicate that all the Cu^{2+} released immediately bind with the nutrients present and precipitate to form crystals.[79] Additionally, Gilbert *et al.* (2012) used high-resolution X-ray spectromicroscopy and high elemental sensitivity X-ray microprobe analyses to reveal that the full intracellular ZnO NP dissolution generated Zn^{2+} that immediately formed complexes with molecular ligands.[116] This NP–protein interaction is able to cause protein misfolding, fibrillation, thiol crosslinking and thus loss of function.[117–119] Interestingly, in a study by Pokhrel *et al.* (2013), the authors developed a model explaining that Zn^{2+} released from ZnO NP dissolution interact with rhombic [2Fe–2S], cuboidal [3Fe–4S], and cubane [4Fe–4S] FeS clusters found in various intracellular proteins, causing changes in cellular responses as a result of the reduced enzymatic activity.[42,120,121] Specifically, NP-induced ROS production is able to damage the highly oxidation-sensitive $[4Fe–4S]^{2+}$ cluster found in the aconitase protein family,[122] generating the intermediate $[4Fe–4S]^{2+}{}^{\bullet}OO^{2-}$. This resulting species reacts with free protons and releases Fe^{2+} to produce $[3Fe–4S]^{3+}$, which is then rendered inactive ($[3Fe–4S]^{0}$) upon univalent reduction.[123,124] Concurrently, Ag^{+} have been shown to complex with Cl^{-}, Br^{-} and thiol-containing biomolecules leading to further damage to cellular functionality.[125–127] Using SR-XANES, Wang *et al.* (2015) revealed the chemical transformation of Ag NPs – as a result of surface oxidation by ROS and dissolved O_2 – from Ag(0) to Ag_2O, which then interacts with organic acid molecules to form AgS.[80] Major sources of intracellular thiol include cysteine and methionine-containing peptides, proteins and antioxidants (*i.e.* MTs), which complex with Ag NPs to form more stable entities.[63,128,129] In fact, the presence of Ag NPs caused a 5-fold and 10-fold increase in the mRNA expression of MTs after 12 h and 24 h, respectively, while circular dichroism spectra revealed alterations in the secondary structures of these antioxidants.[63,80]

2.2.3. A predictive model of NP toxicity based on its dissolution profile. There are various parameters that regulate NP dissolution, including ionic strength, dissolved O_2 concentration and complexing ligands, surface coating, shape and size.[130–133] For instance, NP size is typically inversely correlated with Ag NP dissolution, with the larger surface-to-volume ratio of smaller particles accounting for greater instability and increased solubility.[9] In fact, one method of predicting the toxicity levels of MO NPs is examining specific characteristics including their oxidation number (Z), ionic potential (IP), surface reducibility (SR) and redox reactivity (RR). Based on the above listed physical–chemical parameters, a Bayesian classification system has been established by Simeone *et al.* (2019), in which they assign different categorical variables for each of the parameters mentioned above to determine the conditional probabilities of the cytotoxicity induced by MO NPs over a range of EC_{50} values.[134] Increasing Z represents the strengthening of the electrostatic interactions within the NP structure and thus lowers the degree of NP dissolution, with oxides of M^{z+} with $Z \leq 2$, for instance, dissolving more than 10% of the structure while <1% is dissolved for cationic metals of $Z > 3$. NP surface charge is a key determinant of the level of NP interaction with biological media, particularly in the formation of the protein corona, and it has been repeatedly reported that positively charged NPs are preferentially taken up into cells compared with their negatively charged counterparts.[132,133] Particle surface charge is mainly characterized by its acidity or IP, which is expressed as the ratio of Z to its ionic radius (r) and indicates the extent of hydrolysis. IPs of ≤3 and >5 lead to hydrated and deprotonated surface groups, respectively. SR delineates the type of NP surface defects and describes the MO as reducible or oxidizable according to the potential decrease or increase in M^{z+} oxidation number, respectively.[135] The final parameter RR categorizes NPs with redox potential <−0.8 V (against the standard hydrogen reduction potential at physiological pH) as "non-active", while NPs with higher values were considered "active" and are thus capable of being reduced by GSH or oxidized by dissolved O_2. According to this system, CuO NPs are classified as "highly toxic" due to their low Z (<2), low IP (≤3), surface reducibility, and "active" RR. ZnO NPs are similarly considered highly toxic due to their low Z and IP, although they are "non-reducible" and

"non-active". Both of their high toxicities are mainly attributed to the high likelihood of M^{z+} bioavailability as result of their low *Z*. Within this classification system, the size factor is not incorporated into their assumptions. However, they explain that the chemical mode of interaction with the biological system is not affected, although the probability of this interaction can be increased due to particle size. Furthermore, the effect due to size is difficult to determine as particles can aggregate or dissolve upon interaction with the biological system, resulting in an effective size change. Long-term toxicities caused by aggregation are also not included in this model.

3. Controlling NP dissolution for selective tumor therapy

Selective tumor therapy can thus be achieved by engineering NPs that are responsive to the low pH surrounding tumor tissue and that generate sufficient levels of ROS to induce apoptotic responses in CCs with high metabolic rates, while the additional ROS experienced by normal peripheral cells with higher physiological pH and lower metabolic rates should not reach apoptotic thresholds and only cause temporary reversible damage (Fig. 3). Several methodologies have already been explored to tune the toxicity profiles of the NPs by controlling their distribution, dissolution and oxidative capacity. For instance, Le *et al.* (2016) conducted a multiparametric evaluation of ZnO NPs with varying physicochemical properties such as size (proportional to calcination temperature), aspect ratio (spheres, grains, rods, or needles), dopants with different concentrations (Fe, Mn, or Co), and coatings (polymethylmethacrylate PMMA, silica, oleic acid OA, or serum protein) and assessed their effect on human umbilical vein endothelial cells (HUVECs) and hepatocellular liver carcinoma (HepG2) cells using three toxicity endpoints, including viability, membrane integrity and oxidative stress.[136] The objective of this study was to determine the parameters that have the greatest impact on toxicity and subsequently develop computational models that would be able to predict NP behavior. The descriptors used for the doping elements were similar although not identical to those described above by Simeone *et al.* (2019), and include IP, conduction band energy (EC), and reduction potential (RP). With respect to cell viability, the parameters that had the greatest impact include NP concentration and size, extent of NP shielding from surrounding (solubility and coating type), and the resulting change in IP and EC associated with doping, particularly for Mn-doped oxides which had the largest cytotoxic effect, in contrast to serum-coated NPs that enhanced cell viability. Next, membrane damage was measured by the amount of lactate dehydrogenase (LDH) released, and was shown to be significantly affected by IP, EC, and RP, as well as NP shape, size, solubility and zeta potential. Specifically, in line with previously reported studies, positively-charged NPs exhibited higher LDH release compared to their negatively-charged counterparts, possibly due to the greater interaction of the cationic NPs with the abundant negative residues on cell membranes. Finally, antioxidant response elements (AREs) were used as markers for oxidative stress and were shown to be most affected by the dopant descriptors IP, EC and RP, particularly as a result of Mn- and Co-doping. However, in the context of selective cancer therapy using ZnO and CuO NPs, given that these particles in their bare form already exert the toxicity required for apoptosis in most cell lines as will be discussed in

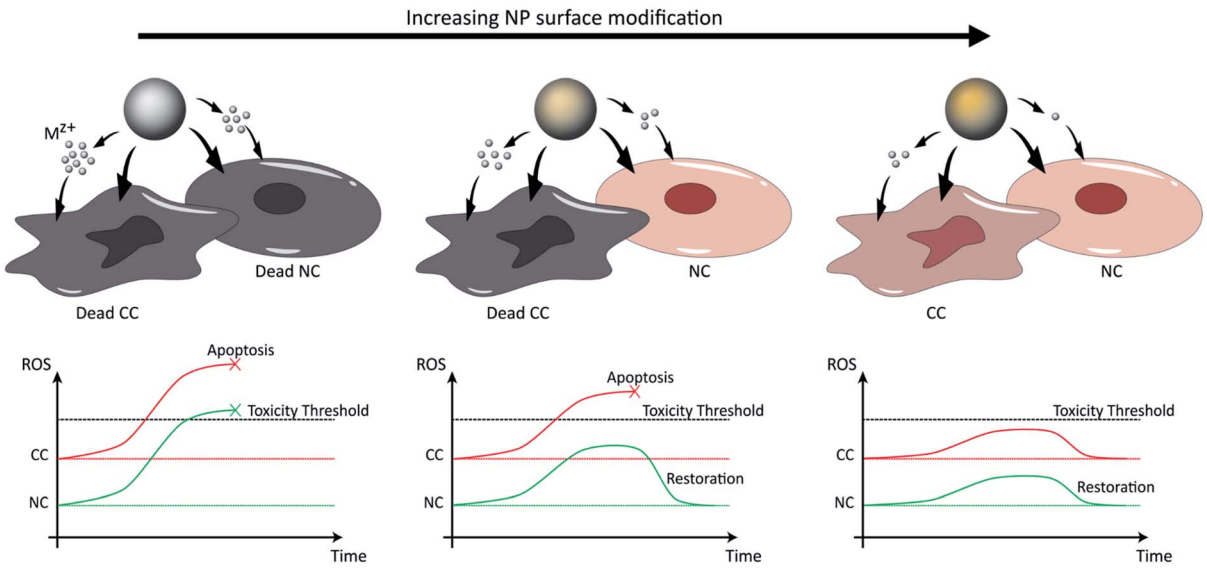

Fig. 3 NP dissolution kinetics and associated toxicity can be tuned by surface modification, including doping and coating, and are increased in the low pH tumor microenvironment. In the first scenario (left), pure NPs release high concentrations of ions that induce ROS generation at levels exceeding toxic thresholds for both CCs and NCs. In the second scenario (right), the excess surface modification of NPs causes a slow release of M^{z+} at non-toxic amounts, preserving the viability of both cell types. Finally, in the third scenario (middle), the M^{z+} release associated with specific extents of NP surface modification is sufficient to exceed toxic thresholds in CCs that possess high metabolism (higher basal levels of ROS), but low enough to exert only transient damage in NCs with low metabolism and to restore oxidative balance.

Section 4, doping them with elements such as Mn and Co that further induce cellular toxicity does not serve the purpose of reducing the impact on NCs. In contrast, doping these NPs with elements such as Fe reduces their dissolution kinetics and associated toxicity, which provides an opportunity to maintain the viability of normal tissue while only exceeding toxic thresholds in the highly metabolic CCs.

3.1. The effect of NP doping on dissolution properties

Doping the NPs with various elements leads to modifications in their electronic state density, magnetic moments, charge distribution, and lattice distortions, altering their reactivity, stability and various other properties. Given that kinetic factors hinder the incorporation of dopants into the NP structure, effective doping is only achieved when the growth rates of the host and dopant are balanced.[137] In this way, the dopant properly substitutes the host core atoms rather than simply adsorb onto the NP surface. In an early work by Bilecka *et al.* (2011), ZnO NPs were doped with Fe, Mn, Ni, Co and V, and the greatest doping efficiency was found for Fe and Co due to their comparable reactivity and size of their divalent ions with Zn.[138] Vanadium, however, had the least effective doping (<3% of dopant precursor content) as it has a larger ionic radius and is a much harder Lewis acid compared with Zn.

As a result, Fe-doping has been heavily explored for ZnO and CuO NPs, and has been shown to significantly reduce particle dissolution and cytotoxicity at levels proportional to the extent of doping,[92] although the toxicity reduction mechanisms for both NP types differ. Within the CuO NP structure, Cu resides among two and four oxygen ligands in the apical and planar positions respectively, which result in Jahn–Teller distortions upon Fe-doping as well as $CuFe_2O_4$ spinal formation.[139] The resulting increased structural stability and surface spinal formation hinders excess Cu^{2+} release. In Fe-doped ZnO NPs, the increased stability compared with pure ZnO is due to the stronger structural binding of Fe than Zn to O, while the Fe atoms simultaneously serve as kinetic constraints for Zn release.[140,141] It has also been suggested that the additional cytoplasmic Fe^{2+} availability originating from the Fe-doped ZnO NPs is able to reduce the previously mentioned oxidized FeS clusters to reverse the protein inactivation process by regenerating the active $[4Fe–4S]^{2+}$ cluster.[42] These reports were further supported by an experiment conducted in *E. coli* that reveal that unstable $[4Fe–4S]^{2+}$ clusters tend to form inactive $[4Fe–4S]^{+}$, and subsequent exposure to Fe ions and dithiothreitol leads to protein reassembly with a 60% gain in protein activity within the span of a few minutes.[142] Therefore, this mechanism of protein function salvaging may also contribute to the reduced cytotoxicity observed with Fe-doped NPs compared to their pure counterparts. Additionally, doping MOs results in the narrowing or expansion of the NP band structure and changes in the positioning of the conduction band edges, altering the levels of ROS generation.[99]

In a recent study from our group investigating the effects of varying Fe doping levels on CuO NP toxicity and cancer therapy, we found that the rapid release of Cu^{2+} from pure CuO causes cell death in both normal and tumor cells, whereas a too slow release leaves both cell types mostly unaffected.[79] By adjusting the Fe-doping levels to fit the exact desired release kinetics of the M^{z+}, it was possible to selectively target CCs. The most beneficial response was achieved at Fe doping levels of 6%. Although the release rate of 6% Fe-doped CuO NPs was initially rapid and overlapped with that of pure CuO, it significantly diminished with time, leading to a slow long-term release (Fig. 4a and b). This decrease in dissolution rate is due to the strong Jahn–Teller distortion that adjusts the planar and apical Cu–O bond lengths. In fact, a 10% Fe-doping of CuO has been previously associated with a 6.4% plane elongation and 4.1% distortion compared to pure CuO.[139] Our EPR spectra showed a Cu release of ~65% from pure CuO and only 8% from 10% Fe-doped CuO in the first 10 minutes of NP exposure to cell culture medium. Using powder diffraction, Rietveld analysis and EDX spectroscopy, we suggested that dissolution causes a transformation from $CuO \rightarrow CuFe_2O_4 \rightarrow Fe_3O_4$ as well as the formation of Fe–O (Fig. 4e and f). Taking into account several assumptions, such as a dissolution rate that is proportional to the surface Cu concentration which itself is proportional to the active surface area for instance, we developed a two-step model to describe the dissolution kinetics of Fe-doped CuO (Fig. 4g). The first step involves the repeated Fe redistribution on the NP surface during Cu^{2+} release and thus a continuous increase in the Fe/Cu surface ratio until all the surface Cu is released, forming an Fe shell. This step is followed by the slow solid-state diffusion of the core Cu to the surface until all the Cu has been released. The remaining Fe particles are then degraded into their ionic form (*i.e. via* Fenton reactions, enzymes[44]), which are then incorporated into the natural Fe metabolism of the cell with the help of ferritin. In fact, this Fe integration has been evidenced through the radioactive labeling of magnetic FeO NPs and the subsequent localization of labeled Fe within the hemoglobin of newly-developed erythrocytes *in vivo*.[22] Therefore, given the safety and success of Fe doping in controlling M^{z+} release and reducing NP cytotoxicity, efforts have been made to test various core-dopant combinations for selective tumor therapy, such as Zn-doped CuO NPs, which have shown to have significant anticancer properties *in vitro* and *in vivo*. These findings will be discussed further in Sections 4 and 5.

3.2. The effect of NP coating on dissolution properties

Besides doping, surface modification of NPs using a wide variety of coatings have also been heavily investigated for their potential in controlling the dissolution kinetics of NPs. For instance, given that silica is highly stable in neutral and acidic environments, a silica coating has been developed around ZnO NPs with the aim of reducing NP degradation and toxicity.[143] This strong hydrophilic coating turns the previously positively-charged surface of the ZnO NPs negative, and the absolute increase in the zeta potential enhances NP stability in water. Optimizing the amount of silica coating could thus result in ZnO NPs with specific degradation profiles. In two separate

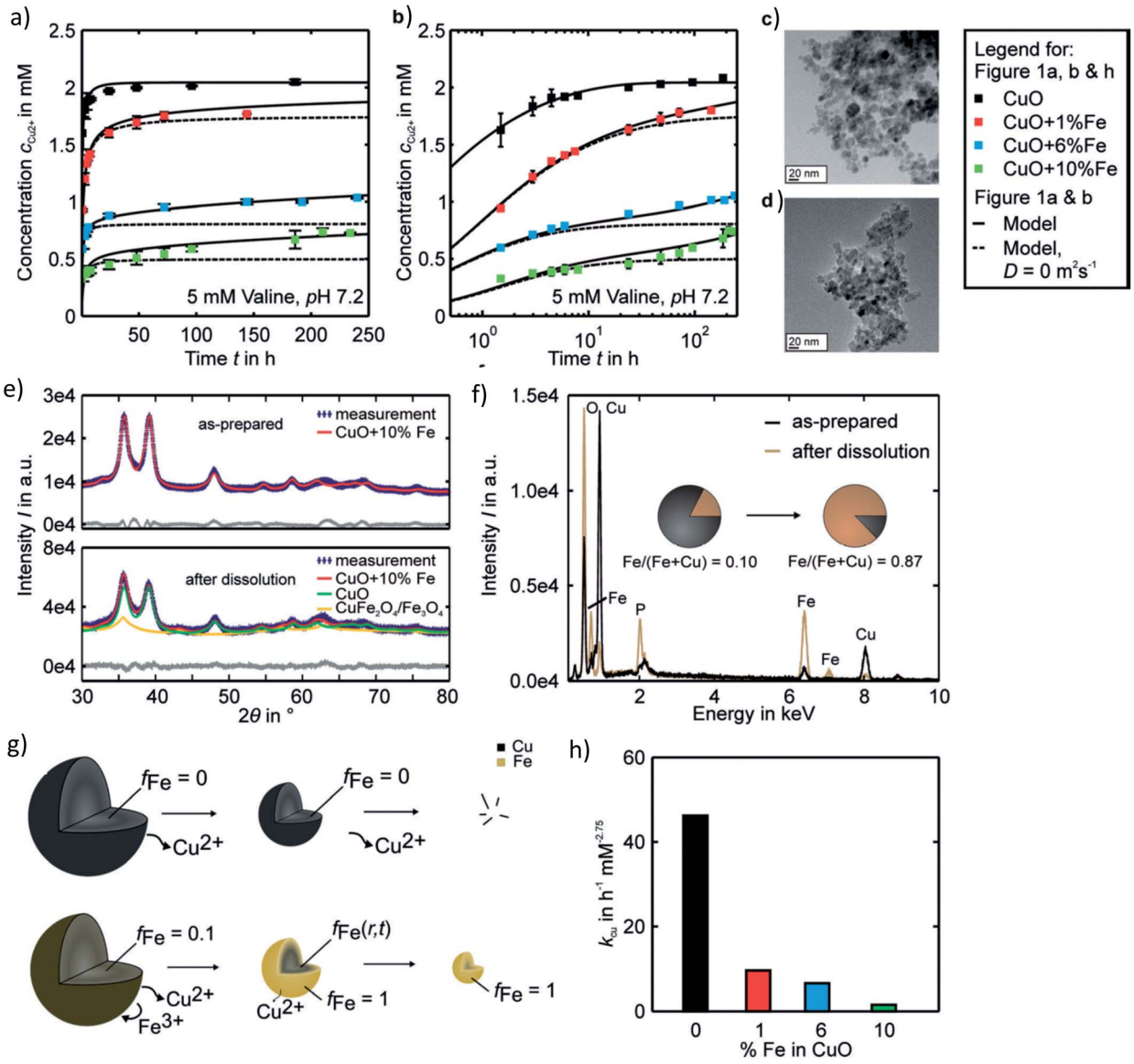

Fig. 4 Pharmacokinetics of Fe-doped CuO NPs as described by Naatz *et al.*[79] (a and b) Cu^{2+} release profiles showing a slow long-term release in the case of the higher doped NPs in the logarithmic time scale. (c and d) TEM images of 10% Fe-doped NPs before and after dissolution in the span of 4 weeks. (e and f) Powder diffraction patterns and EDX spectra depicting the change in particle composition before and after dissolution of the 10%-doped CuO NPs. (g) Proposed two-step model of Fe-doped CuO NP dissolution wherein all the surface available Cu is first released until an Fe shell forms, followed by the solid-state diffusion of core Cu to the surface until all the particle Cu is removed. (h) Decrease in the dissolution rate constants with increasing Fe doping. This image has been reproduced with permission from Naatz *et al.*,[79] © Wiley-VCH, 2020.

studies, other types of surface coatings were assessed on either CuO[144] or ZnO[145] NPs with the aim of completely reducing the surface reactivity and M^{2+} release from the particles. Osmond-McLeod *et al.* (2013) demonstrate almost full reduction of ZnO NP toxicity as a result of surface coating them with dimethoxy-diphenylsilane/triethoxy-caprylylsilane cross-polymer (MAX) compared to pure ZnO.[145] However, coating the NPs with triethoxycaprylylsilane (HP1) resulted in moderate cytotoxic response. Given that the aim of the study was to fully reduce NP dissolution as a safety measure and as a result, the HP1-coated NPs were not further investigated, these findings suggest the need to further test the HP1-coated NPs for the purposes of cancer therapy by tuning their dissolution kinetics. Similar conclusions can be derived from the study by Cai *et al.* (2017), who show that after coating with ethylenediamine tetra (methylene phosphonic acid) (EDTMP), the extent of CuO dissolution was less than 0.2% and almost no ROS generation and toxicity were observed in THP-1 and BEAS-2B cells.[144] They also report that the coating does not disrupt the CuO crystal structure and morphology. Meanwhile, they tested the impact of coating NPs with citrate and PVP (polyvinylpyrrolidone), which had limited and moderate protective effects, respectively. Similarly to the case of HP1-coated ZnO NPs, optimizing NP dissolutions profiles may be achieved by investigating varying

degrees of NP coating with PVP. A follow-up study by Líbalová *et al.* (2018) revealed that varying NP surface modifications (anionic sodium citrate CIT, sodium ascorbate ASC, neutral PVP, cationic polyethylenimine PEI) only moderately affected Cu^{2+} release and that the toxicity observed in a murine macrophage cell line was mainly determined by the NP coating agent and Cu bioavailability rather than the intracellular Cu burden, with the PEI-coated NPs being the most toxic.[47]

4. Cellular studies on cancer-specific NP toxicity *in vitro*

Although a few types of doping and coatings were introduced in the previous section, there exists a variety of other surface materials that have been experimented with in order to fine tune the dissolution kinetics of NPs. In this next part, we initially discuss the various studies that have tested the anticancer activity of pure ZnO, CuO, and Ag NPs *in vitro*, followed by the efforts that have been made over the years to further enhance CC selectivity using the assorted doping and coating materials and their cellular responses. Please note that a wide range of different cell types have been used in the various studies, which will not be described in detail as this would be outside of the scope of the current manuscript. For clarity purposes, we have listed all cell types described with their abbreviation and full name in Table 1. A summary of all the discussed studies is also provided in Tables 2–4.

4.1. CC-specific toxicity of pure NPs

4.1.1. ZnO NPs. Throughout the years, ZnO NPs have been tested for their toxicity in a variety of cell types and have clearly demonstrated selective anticancer properties *in vitro*. In an early study by Akhtar *et al.* (2012), the underlying mechanisms of ZnO NP cytotoxicity were investigated in three human CC lines and two primary rat cell lines (astrocytes and hepatocytes).[89] The NPs were shown to selectively kill CCs without having an impact on normal tissue, and subsequent molecular data demonstrated that the toxicity mechanisms include the upregulation of mRNA and protein levels of *p53* and *bax*, as well as the downregulation of *bcl-2*. Moreover, ZnO NPs induced the activation of caspase-3 and DNA fragmentation as a result of ROS generation and oxidative stress. In a similar study, two different ZnO NPs – green- and yellow-green-emitting – were shown to have selective cytotoxic impact on human CC lines including HepG2, leukemia K562 and K562/A02.[146] Increasing the concentration of these NPs directly impacted their cellular uptake and thus, toxicity. Hassan *et al.* (2017) also reported enhanced toxicity associated with increasing ZnO NP concentration in three human CC lines (HepG2, prostate cancer PC3, and lung adenocarcinoma A549), although the absolute toxicity levels differed between cell types.[147] Additionally, in a study comparing the effects of Al_2O_3, TiO_2, CeO_{2-x} and ZnO NPs on A549, NCI-H460 (hypotriploid cell line), SK-MES-1 (lung CC line), HeLa, and Jurkat (T-lymphocytes to study T-cell

Table 1 Cell types referred to in the discussed studies and their abbreviations

Cell line	Type	Cell line	Type
A172	Human glioblastoma	KCL22	Human chronic myeloid leukemia
A549	Human lung adenocarcinoma	KLN205	Murine lung carcinoma
AsPC-1	Human pancreatic tumor	L02	Human hepatic
B16	Murine melanoma	L5178Y-R	Murine lymphoma
BEAS-2B	Human lung epithelial	LS174T	Human colon cancer
BeL7402	Human hepatocellular carcinoma	MCF-7	Human breast cancer
BJ	Human normal fibroblasts	MCF-7/ADR	MCF-7 adriamycin-resistant (ADR)
BxPC-3	Human pancreatic cancer	MDA-MB-231	Human breast cancer
C6	Rat glioma	MG-63	Human osteosarcoma
CHO	Chinese hamster ovary epithelial	MIA Paca-2	Human pancreatic cancer
COLO 205	Human colon adenocarcinoma	MSC	Mesenchymal stem cells
CT26	Murine colorectal carcinoma	N417	Human small cell lung cancer
DAL	Canine hemangiosarcoma	NCI-H460	Human non-small lung cancer
EAC	Murine Ehrlich Ascites carcinoma	NIH3T3	Mouse embryonic fibroblasts
ESC	Embryonic stem cells	OUS-11	Human lung normal
H1299	Human non-small lung cancer	PANC1	Human pancreatic cancer
H187	Human small cell lung carcinoma	Panc28	Human pancreatic adenocarcinoma
H82	Human small cell lung carcinoma	PBMC	Peripheral blood mononuclear cells
HCC	Human hepatocellular carcinoma	PC3	Human prostatic cancer
HCT116	Human colorectal carcinoma	RAW264.7	Murine macrophage
HeLa	Human Henrietta Lacks immortal cells	SHSY5Y	Human neuroblastoma
HepG2	Human liver hepatocellular carcinoma	SK-MES-1	Human lung cancer
HT-29	Human colon cancer	SKBR3	Human breast cancer
HT1080	Human fibrosarcoma	SUM159	Mesenchymal TNBC
hTERT-HPNE	Immortalized human pancreatic duct	TNBC	Triple-negative breast cancer
HUVEC	Human umbilical vein endothelial	U251	Human glioblastoma
Jurkat	Human immortalized T lymphocytes	U87	Human primary glioblastoma
K562	Human myelogenous leukemia	WI38	Human lung fibroblasts
K562/A02	Human leukemic	WISH	Human amnion

Table 2 Summary of *In vitro* and *in vivo* studies testing the effects of pure and surface-modified ZnO NPs[a]

Surface mod.	Size (in nm)	Main finding	VT	VV	Model systems	Dose/concentration	Cellular/tumoral effects	CCS	Mechanism	Ref.
Pure	21^{C}, 131^{HD}	ZnO NPs selectively induce apoptosis in CCs *via* ROS, mediated by p53, bax/bcl-2 and caspase pathways	●		HepG2, A549, BEAS-2B, rat astrocytes & hepatocytes	5–15 μg mL^{-1}	Dose-dependent ↓ cell viability	●	↑ *p53* and *bax* and ↓ *bcl2*	89
Pure	5^{C}, 6^{C}	Newly synthesized ZnO QDs with promising optical properties show cytotoxic effects in CC lines	●		K562, K562/A02, HepG2	1.25–100 μg mL^{-1}	Dose-dependent ↓ cell viability			146
Pure	35^{C}	ZnO NPs restore oxidative balance, hepatocyte integrity and tumor markers to normal levels in HCC	●	●	VT: HepG2, PC3, A549; VV: HCC	VT: 0–1000 μmol L; VV: 10 μg kg^{-1} per week	Dose-dependent ↓ cell viability		Restoration of oxidant and antioxidant activity (MDA, GSH, GPx, GSR, SOD, CAT), hepatocyte integrity (ALT, AST, LDH) and tumor biomarkers (AFP, AFU) to normal levels in CCs	147
Pure	95^{HD}	ZnO NPs exert toxicity in normal and CCs through ROS generation, whereas CeO_2 and TiO_2 NPs do not	●		A549, NCI-H460, SK-MES-1, HeLa, Jurkat, AT II	2–6 μg cm^{-2}	↓ cell viability		Complete particle dissolution and ↑ ROS	57
Pure	100^{HD}	ZnO and Ag NPs evoke stress-induced autophagy in pulmonary and hepatic cells while TiO_2 NPs do not	●		A549, HepG2	1–500 μg mL^{-1}	Dose-dependent ↓ cell viability		Autophagy induction (↑ *LC3B*, *atg4b*, *p62* and ↓ *atg12*, *atg5*) in a time-dependent manner, and apoptotic cell death *via* caspase-3	148
Pure	40^{C}	Apoptosis and oxidative stress as relevant mechanisms of antitumor activity and genotoxicity of ZnO-NPs		●	ESC	50, 300 and 500 mg kg^{-1} per body weight			Oxidative stress (↑ MDA and ↓ CAT, GST) and DNA damage. Apoptosis (↑ Bax and p53, ↓ Bcl2). NAC restores oxidative balance in the liver and kidney without ↓ the antitumor efficacy of NPs	184
Pure	20^{HD}, 70^{HD}	Genotoxic anticancer effects of ZnO NPs *via* ROS, leading to non-apoptotic cell death in an orthotopic mouse model of human small-cell lung cancer	●	●	VT: H82, H187, BEAS-2B, MCF-7, OUS-11, LS174T, N417; VV: N417	VT: 0–20 μg mL^{-1}; VV: 0.04–0.25 mg kg^{-1}	Dose-dependent ↓ cell viability. ↓ tumor density	●	↑ ROS and DNA leakage from nuclei. Phos. of CHK2 in N417 and LS174T cells. ↑ cleaved PARP in LS174T cells. Q-VD-OPh (inhibitor of caspase-3, 1, 8, 9, slightly ↑ viability by inhibiting apoptosis, but did not block ZnO toxicity)	185

Table 2 (*Contd.*)

Surface mod.	Size (in nm)	Main finding	VT	VV	Model systems	Dose/concentration	Cellular/tumoral effects	CCS	Mechanism	Ref.
Fe-doped (0–10%)	20.2^{C}–8.3^{C} (0–10%)	Fe doping reduces ZnO toxicity in animals due to decreased NP dissolution rates and associated toxicological responses	●	●	VT: RAW264.7, BEAS-2B; VV: rat & mouse lung, zebrafish embryo	VT: 12.5 μg mL^{-1}; VV: 0–50–150 μg mL^{-1}	↓ toxicity with ↑ Fe doping		↑ Fe doping leads to ↓ inhibitory effect of Zn^{2+} in zebrafish embryo hatching, ↓ PMN cell counts in the BAL fluid and IL-6 mRNA and ↑ heme oxygenase 1 in mouse lung, and ↓ BAL PMN cell counts, LDH, and albumin in rat lung	163
Fe-doped (0–10%)	11^{C}, 5.5^{C} (0, 10%)	2% Fe-doped ZnO NPs are found to be optimal to cause selective CC death and reduce metastasis formation	●	●	VT: mMSC, Beas-2B, HeLa, KLN205; VV: KLN 205	VT: 0–35 μg mL^{-1}; VV: 125 μg per animal	↓ cell viability. ↓ toxicity with ↑ Fe doping. ↓ tumor growth and metastasis (2, 10%)	●	↑ ROS, membrane and mitochondrial damage and autophagy. ↓ toxicological response with ↑ Fe doping due to resulting ↓ in cellular levels of Zn^{2+}. VV: pure NPs led to weight loss and premature death of mice	77
La-doped (0–5%)	33^{C}, 29^{C} (0, 5%)	Doping ZnO NPs with La increases NP photocatalytic activity and cytotoxicity	●		MDA-MB-231, KCL22, HeLa	6–500 μg mL^{-1}	Dose-dependent ↓ viability. ↑ toxicity with La doping			164
Sm-, Eu-, Gd-doped	$>100^{C}$	Sm-doped ZnO NPs displays the most significant antitumor activity compared to other lanthanide-doped ZnO NPs	●	●	EAC	VT: 0–0.05 mol; VV: 150–350 mg kg^{-1}	Dose-dependent ↓ cell viability for Sm^{3+} : ZnO NPs		Compared to pure NPs, Sm-doping ↓ tumor size, ↓ PI3K, Akt and mTOR, ↓ *CXCR4* and P450, ↓ *Bcl2* : *Bax* ratio, ↓ liver function enzymes (AST, ALT) and induce G2 cell cycle arrest	165
PEG or starch coated	$40–1200^{HD}$	Toxicity towards osteoblast CCs is dependent on NP size, aspect ratio and coating. PEG-capped NPs exhibit higher toxicity than starch-capped NPs	●		MG-63	1 μM to 7 mM	Dose-dependent ↓ cell viability. ↓ toxicity with ↑ NP size			167

[a] ^{C}core size, ^{HD}hydrodynamic size, VT *in vitro*, VV *in vivo*, CCS cancer-cell specific.

Table 3 Summary of *in vitro* and *in vivo* studies testing the effects of pure and surface-modified CuO NPs[a]

Surface mod.	Size (in nm)	Main finding	VT	VV	Model systems	Dose/concentration	Cellular/tumoral effects	CCS	Mechanism	Ref.
Pure	7^{C}, 127^{HD}	CuO NPs inhibit pancreatic tumor growth primarily by targeting TICs *via* ROS and mitochondrial pathway	●	●	PANC1	VT: 0–50 μg mL^{-1}; VV: 0–12.5 mg kg^{-1}	Dose- and time-dependent ↓ cell viability. Tumor growth inhibition	●	↑ ROS, ↓ MMP, apoptosis of TICs (arrest in sub G1 phase)	149
Pure	22^{C}, 167^{HD}	CuO NPs induce mitochondria-mediated apoptosis in human hepatocarcinoma cells	●		HepG2	0–50 μg mL^{-1}	Dose-dependent ↓ cell viability		Oxidative stress (↑ MDA, ↓ GSH) ↑ ROS, DNA damage. Mitochondria-mediated apoptosis (↓ MMP, ↑ P53, ↑ BAX/BCL2 and caspase-3)	150
Pure	20^{C}	CuO NPs induce cytotoxicity *via* mitochondrial pathway	●		K562, PBMC	0–25 mg mL^{-1}	Dose-dependent ↓ cell viability	●	↑ ROS, mitochondria-mediated pathway, ↑ P53 and Bax/Bcl2	151
Pure	30^{C}, 235^{HD}	Autophagy is the main mechanism of CuO NP-induced cell death, while apoptosis is only triggered secondarily	●		MCF7	0–12 μg mL^{-1}	Dose- and time-dependent ↓ cell viability		Autophagy: ↑ MAP-LC3-II, Beclin1 and ATG5. 3 MA inhibits autophagy, and further Beclin1 KD leads to apoptosis (↑ PARP-cleavage, BAD dephosphorylation and caspase-3)	95
Pure	12^{C}	CuO NPs synthesized from *Eucalyptus globulus* induce apoptosis in breast carcinoma	●		MCF7	0–100 μg mL^{-1}	Dose-dependent ↓ cell viability		Impaired MMP, ↑ ROS, ↑ p53, bax, caspase-3, and caspase-9, cell cycle arrest in G1, S and G2/M phases	90
Fe-doped (0–10%)	11.8^{C}–10.7^{C} (0–10%)	6% Fe-doped CuO NPs induce inhibition of tumor growth and complete tumor remission when combined with immunotherapy	●	●	VT: MSC, Beas-2B, HeLa, KLN205; VV: KLN205	VT: 0–35 μg mL; VV: 0–225 μg kg^{-1} bw (6%)	↓ toxicity with ↑ Fe doping. ↓ tumor growth (6%-doped)	●	↑ membrane damage, ROS, autophagy. ↓ toxicity with ↑ Fe doping. VV: ↑ local antitumor immune response (activation of CD8+ and NK cells). Complete tumor remission due to treatment with 6%-doped NPs and EPAC	79
Fe-doped (10%)	235^{HD}, 247^{HD} (0, 10%)	Fe-doping of CuO NPs lowers their toxic potential on glioblastoma cells by slowing down Cu release	●		C6	0–1000 μM	Dose- and time-dependent ↓ cell viability. ↓ toxicity with ↑ Fe doping		↑ ROS and oxidative stress. Cu chelators can prevent Cu-induced toxicity	168

Table 3 (*Contd.*)

Surface mod.	Size (in nm)	Main finding	VT	VV	Model systems	Dose/concentration	Cellular/tumoral effects	CCS	Mechanism	Ref.
Zn-doped	30[C]	Zn–CuO NPs exert selective antitumor activity (inhibition of glioblastoma growth) and reverse temozolomide resistance in glioblastoma by inhibiting AKT and ERK1/2	●	●	VT: Panc28, HCT116, U87, C6, HELA, BeL7402, U251, A172, HUVEC, NIH3T3; VV: U87	VT: 5.0–20.0 μg mL^{-1}; VV: 0–100 mg kg^{-1}	Dose-dependent ↓ GBM cell proliferation. ↓ tumor growth, cell migration and invasion	●	↑ ROS, apoptosis (↑ procaspase-9, procaspase-3 and ↓ bcl-2/bax ratio), inhibition of AKT and ERK1/2	169
Zn-doped	30[C]	Zn–CuO NPs inhibit pancreatic cancer growth by inducing autophagy through AMPK/mTOR pathway	●	●	VT: AsPC1, MIA Paca2, HepG2, BxPC3, PANC1, HT29; VV: AsPC1	VT: 0–160 μg mL^{-1}; VV: 5 and 10 mg kg^{-1}	Dose-dependent ↓ cell viability. Inhibition of tumor growth		↑ ROS. Autophagy induced *via* AMPK/mTOR pathway (↑ p-AMPK, p-ULK1, Beclin-1 and LC3-II/LC3-I ratio, ↓ mTOR phosphorylation)	170
Zn-doped	2–10[C]	Zn–CuO NPs inhibit tumor growth by NF-κB pathway. NAC restores the balance disrupted by autophagy and apoptosis	●	●	VT: HepG2, Panc28; VV: Panc28	VT: 0–40 μg mL^{-1}; VV: 5 and 10 mg kg^{-1}	Dose-dependent ↑ cell proliferation inhibitory rates		NF-κB signaling involved in ROS-induced apoptosis (↑ Bax and caspase 3, Bcl-2 ↓) and autophagy (↑ LC3B and LC3 B/A). DNA, ER & Golgi damage. All effects restored with NAC	172
Zn-doped	3[C]	Zn–CuO NPs inhibit human CC growth through ROS-mediated NFκB activations	●		HepG2, Bel7402, A549, Panc28, HT1080, Hela, HUVEC, L02	0–60 μg mL^{-1}	Dose-dependent ↑ cell proliferation inhibitory rates	●	↑ ROS and NF-κB pathway activation (↑ p-IKKα/β and nucleus p-NF-κB p65, ↓ IKKα, IKKβ, IκBα and nucleus NF-κB p65 expression). Induction of G2/M cell cycle arrest	171
Carbon (C)-coated	10.4–19.4[C] (CuO–C/Cu)	C-coat decreases cytotoxicity of CuO NPs due to reduced solubility, and CuO NPs induce greater toxicity than Cu^{2+}	●		CHO, HeLa	30 ppm C/Cu, 34 ppm CuO	Dose-dependent ↓ cell viability. ↓ toxicity with C-coating	●		103
Protein coating (DMSA)	141[HD] (pure), 167[HD] (coated)	pCuO-NP-induce cell death in glioblastoma cells to a lesser extent than pure CuO NPs, due to reduced Cu ion release	●		C6, primary astrocytes	0–1000 μM	Dose- and time-dependent ↓ cell viability. ↓ toxicity with protein coat		↓ LDH and ↓ MTT reduction capacity. Cu chelators and low temperature ↓ toxicity	173

[a] [C]core size, [HD]hydrodynamic size, VT *in vitro*, VV *in vivo*, CCS cancer-cell specific.

Table 4 Summary of *in vitro* and *in vivo* studies testing the effects of pure and surface-modified Ag NPs[a]

Surface mod.	Size (in nm)	Main finding	VT	VV	Model systems	Dose/concentration	Cellular/tumoral effects	CCS	Mechanism	Ref.
Pure	8–22[C]	Ag NPs synthesized from plant extracts induce anticancer activity in lung cancer models	●	●	H1299	VT: 2–30 μg mL^{-1}; VV: 10 μg g^{-1}	Dose-dependent ↓ cell viability. ↓ tumor size & growth		Morphological alterations, ↓ NF-κB transcriptional activity and Bcl2, ↑ caspase-3 and survivin	152
Pure	5–35[C]	Bio-synthesized Ag NPs exhibit anticancer, antioxidant and anti-angiogenic activity with no adverse effect on liver and kidney		●	DAL	VT: 0–100 μg mL; VV: 50 μg mL^{-1}	Dose-dependent ↓ cell viability *ex vivo*			187
Pure	9.4–25.9[C]	Ag NPs synthesized from *Nostoc linckia* extracts exert anticancer activity in breast cancer models	●	●	VT: MCF-7, WI38, WISH; VV: EAC	VT: 1.56–100 μg mL^{-1}; VV: 5 mg kg^{-1}	Dose-dependent ↓ cell viability. ↓ cell volume, cell count and weight of tumors	●		153
Pure	31.8[C]	Ag NPs synthesized from *Acorus calamus* show antitumor activity with complete NP elimination 89 days post-treatment	●	●	VT: Hep2, COLO 205, SH-SY5Y	0–200 μg mL^{-1}	↓ cell viability		↑ ROS, ↓ MMP, ↑ caspases-8, 9 and 3, ↑ lamin and PARP, ↑ MDA, ↓ SOD, GPx and CAT	154
Pure	8–20[C]	Ag NPs synthesized from *Agaricus bisporus* cause apoptosis and anti-angiogenesis in combination with gamma radiation	●	●	VT: MCF-7; VV: EAC	VV: 0.1–10 μg kg^{-1}	Dose-dependent ↓ cell viability		↑ caspase-3, ↑ nitric oxide and MDA, ↑ ROS, DNA damage	155
Pure	2.6[C], 18[C]	Ag NPs induce size-dependent cell death in chemo-resistant pancreatic CCs *via* apoptosis, autophagy, necroptosis and mitotic catastrophe	●		PANC-1, hTERT-HPNE	0–5μg mL^{-1} (2.6 nm), 0–100 μg mL^{-1} (18 nm)	Dose-dependent ↓ cell viability. ↓ toxicity with ↑ NP size	●	Apoptosis: ↑ bax, p53, ↓ bcl-2. Necroptosis: ↑ MLKL, RIP1, RIP3. Autophagy: ↑ LC3-II	91
Citrate-coated	5[C]	Ag NPs initiate antitumor effects and trigger the activation of a tumor cell-specific immune response	●	●	VT: HeLa, A549, KLN205; VV: KLN205, CT26	VT: 5–50 μg mL^{-1}; VV: 100 μg	Dose-dependent ↓ cell viability. Tumor inflammation and ↓ tumor size		↑ ROS, mitochondrial damage, autophagy, immunomodulatory effects (↑ NFκB pathway and ↑ IL-1α)	175
PVP-coated	30–50	Ag NPs induce toxicity to CCs *via* necrosis and increase survival of mice	●	●	L5178Y-R	VT: 9–579 nM; VV: 20 mg kg^{-1}	Dose-dependent ↓ cell viability			97
PVP-coated	5–75[C]	Ag NPs show selective cytotoxicity against TNBC cells regardless of size, shape or coating	●	●	VT: TNBC, MDA-MB-231, SUM159; VV: TNBC	VT: 0–60 μg mL^{-1}; VV: 6 mg kg^{-1}	↓ proliferation. ↓ tumor growth rate, ↑ survival rate	●	Impairment of cellular redox balance, ↑ ER stress, UPR activation, ↑ CHOP, DNA damage	178
EPS-coated	11[C]	Ag NPs biogenerated by *Klebsiella oxytoca* DSM 29614 show anticancer activity mainly by induction of autophagy	●		SKBR3	5 and 50 μg mL^{-1}	Dose- and time-dependent ↓ colony-forming ability		↑ ROS. Autophagy: ↑ ATG5, ATG7, LC3-II and Beclin-1, ↓ AKT, p-AKT, p62 and HSP90	177
	<2[C]		●		BJ	62.5, 250 and 1000 mM			Activation of p53	176

Table 4 (*Contd.*)

Surface mod.	Size (in nm)	Main finding	VT	VV	Model systems	Dose/concentration	Cellular/tumoral effects	CCS Mechanism	Ref.
Ag^{+}-R, Ag^{0}-R		Compared to Ag^{+}-R NCs, Ag^{0}-R nanoclusters (NCs) exhibit greater release of Ag species					Toxicity by Ag^{0}-R NCs > Ag^{+}-R NCs		
TAT-coated	8[C]	Antitumor activity in both multidrug resistant and non-resistant CCs is greater with TAT functionalization	●	●	VT: HeLa, MCF-7 (/ADR), B16; VV: B16	VV: 1 nmol kg^{-1}	↓ cell viability. ↓ tumor growth at lower doses than DOX		191

[a] [C]core size, [HD]hydrodynamic size, VT *in vitro*, VV *in vivo*, CCS cancer-cell specific.

Leukemia), ZnO NPs exerted the highest toxicity after a 24 h exposure compared to the remaining NPs which exhibited minimal to no impact, and their subsequent coating with protein coronas significantly improved cell viability.[57] Another comparative study assessing the viability of HepG2 and A549 cells in response to treatment with various NPs showed that the 50% lethality (LC_{50}) was reached for both cell types treated with Ag and ZnO NPs as well as increased caspase-3 expression levels, whereas minimal toxicity was observed in TiO_2 NP-treated cells.[148]

4.1.2. CuO NPs. As with ZnO NPs, CuO NPs have been heavily investigated as anti-cancer therapeutic agents in a wide variety of cell lines. In human pancreatic CC (PANC1) cultures enriched with tumor initiation cells (TICs), a considerable decrease in cell viability was found upon CuO NP treatment compared with standard PANC1 cultures.[149] TICs are a subpopulation of CCs with stem cell properties, which are highly resistant to most of the current treatments and are therefore assumed responsible for tumor regrowth after therapy. Underlying mechanisms of their therapeutic resistance are linked to ROS scavenging, as lower ROS levels are exhibited in TICs compared to other cells in the tumor tissue. Interestingly, however, administration of CuO NPs was able to induce elevated levels of ROS and oxidative stress in TICs, leading to mitochondrial damage and apoptosis.

Similarly to the previously reported findings concerning the cytotoxic effects of ZnO NPs, CuO NPs were found to have a dose-dependent (DD) toxic effect on HepG2 (ref. 150) and K562 (leukemia)[151] cells in two separate studies, and were associated with the upregulation of *p53*, increased ratio of BAX/BCL2, and decrease in MMP, suggesting that a mitochondria-mediated pathway is involved in CuO NP-induced apoptosis. Expression levels of *caspase-3* were also measured in the HepG2 cell line and were found to be elevated. Multiple studies have also tested the effects of CuO NPs in human breast CCs. In the MCF7 cell line, CuO NPs induced dose- and time-dependent autophagy as a possible defence mechanism against CuO-induced toxicity.[95] Apoptosis-related cell death was indicated by PARP cleavage, bcl2-associated death promoter (BAD) dephosphorylation and increased caspase 3 cleavage. A more recent *in vitro* study on MCF7 cells by Ali *et al.* (2020) used CuO NPs synthesized from *Eucalyptus globulus* leaf extract (ELE) with anticancer and antifungal activity.[90] They demonstrated a considerable reduction in cell survival *via* an impairment of MMP and elevation in intracellular ROS. Cell cycle analysis indicated disruption/arrest in different phases (G1, S and G2/M phases) upon CuO NP administration, leading to apoptosis. This data was further confirmed by the upregulated expression levels of *p53*, *bax*, *caspase-3*, and *caspase-9* genes.

4.1.3. Ag NPs. Dose-dependent toxicity in a variety of cell lines has also been observed in the context of Ag NPs. For instance, studies testing the effects of Ag NPs on human lung cancer (H1299)[152] and MCF-7 cells[153] showed a DD decrease in viability. In the H1299 cells, induction of apoptosis, confirmed by the assessment of morphological characteristics such as cell shrinkage and nuclear condensation also displayed such a relationship.[152] As seen with ZnO and CuO NPs, a decrease in

bcl2 and NF-κB transcriptional activity was detected, alongside an increase in both caspase-3 and survivin levels. In the MCF-7 cells, a lower IC_{50} value was obtained as compared to two NC lines – human lung fibroblast cells (WI38) and human amnion cells (WISH) – further highlighting the selective antitumor properties of Ag.[153]

With the aim of circumventing the use of toxic and expensive chemicals, Nakkala *et al.* (2018) synthesized Ag NPs using a green pathway (rhizome extract of *Acorus calamus*), and these NPs significantly impacted the viabilities of different CC lines, including Hep2 (human epidermoid carcinoma), COLO 205 (human colon adenocarcinoma) and SH-SY5Y (neuroblastoma).[154] Hep2 cells, which clearly showed lower IC_{50} values after 24 h, displayed characteristics of late apoptosis such as the rounding up of nuclei, cell shrinkage, nuclear condensation and fragmentation, and loss of MMP. Furthermore, an increase of ~66% in ROS levels and 1.2-fold in MDA levels (marker of oxidative stress), as well as a decrease in SOD, GPx and CAT antioxidant activity were detected. It was thereby concluded that both intrinsic and extrinsic apoptotic pathways are involved in the cell death of Ag NP-treated cells. Other biologically-synthetized Ag NPs were also shown to induce a DD reduction in viability in MCF-7 cells.[155] The selectivity of Ag towards CCs was further highlighted in a study by Zielinska *et al.* (2018), wherein 2.6 and 18 nm Ag NPs exerted higher cytotoxicity against PANC-1 CCs compared to non-tumor cells of the same tissue (hTERT-HPNE cells).[91] Both Ag NPs induced, in a size- and concentration-dependent manner, a significant decrease in proliferation and cell death after 24 h, which appeared to be regulated by apoptosis, necroptosis, autophagy and/or mitotic catastrophe as a result of alterations in the protein levels associated with each mechanism. The role of apoptosis in Ag NPs-induced PANC-1 cell death was confirmed by significant increases in the levels of BAX and P53 and very low levels of BCL2. Evidence for necroptosis and autophagy was shown by a size- and concentration-dependent increase in MLKL, RIP1 and RIP3 protein levels and an increase in LC3-II, respectively. Finally, the role of mitotic catastrophe in Ag NPs-induced cell death was confirmed by the observed increase in cell size combined with multinucleation.

4.1.4. IONPs. Various IONP formulations have been clinically approved as MRI contrast agents, Fe replacement strategy or as mediator for magnetic hyperthermia in cancer therapy.[156] While IONPs are therefore used in cancer therapy, and furthermore are known to degrade in a pH-dependent manner, this degradation has thus far not been linked to a cancer-selective toxicity, to our knowledge. Fe is essential to many biological functions.[157] However, much like other MO NPs, the redox properties of IONPs which are intimately associated to its activity with proteins can potentially give rise to toxicity. The presence of ferric ions in the degradative environment of lysosomes can lead to the production of free oxide radicals due to the Fenton reaction, which can cause substantial toxicity when intracellular concentrations of IONPs are exceeded. This degradation followed by the Fenton reaction has been shown to be particularly affecting cells of neuronal lineage, as was first demonstrated by Pisanic and colleagues.[158]

IONPs have been shown to induce some interesting effects, linked to their degradation, which are unique among the other NPs. Firstly, when relatively low levels of IONPs are used, the released ferric ions can promote cell proliferation, as demonstrated for mesenchymal stem cells, as Fe is a vital component in cell cycle progression.[159] Secondly, upon degradation of IONPs, it has been shown that they keep evolving with time. Initially, they undergo a rapid burst of degradation, after which ferric ions are transported to ferritin for long-term storage under its ferrihydrite form ref. 160 and 161. It has been shown that stem cells can however resynthesize novel biogenic IONPs with a magnetite structure.[162]

4.2. Effect of NP doping and surface modification on cellular toxicity *in vitro*

4.2.1. Metal-doped or coated ZnO NPs. Although the pure forms of the NPs have been shown to have intrinsic anticancer properties, this selectivity towards CCs can be further optimized by controlling the dissolution kinetics of the NPs. As previously mentioned, one method of fine-tuning M^{z+} release is by doping these NPs with other metals. Specifically, Fe doping exhibits high efficiency in lowering cytotoxicity in a dopant concentration-dependent manner. An early study on Fe doping demonstrated that the toxicity profiles of 1, 2, 4, 6, 8 and 10% Fe-doped ZnO NPs in RAW264.7 (mouse macrophages) and BEAS-2B (human bronchial epithelial) cells showed a progressive decline in all tested toxicological responses with increasing levels of Fe doping due to reduced dissolution rates.[163] Later in 2017, a similar conclusion was made by Manshian *et al.* when testing the same set of Fe-doped ZnO NPs on normal murine mesenchymal stem (mMSCs) and BEAS-2B cells, as well as on murine lung squamous carcinoma (KLN205) and human cervical cancer (HeLa) cells.[77] They assessed the rate of dissolution of this NP series and found that NPs with no (0%) or low (1% and 2%) Fe-doping showed a significantly higher dissolution rate in CCs compared to NCs, possibly due to the higher metabolic rates and acidic environments associated with CCs. Using high-content imaging, they assessed cellular parameters such as viability, membrane damage, mitochondrial ROS generation and health, among others, and found a clear negative correlation between the degree of Fe-doping and the level of toxicity in a concentration-dependent manner. They further confirmed the higher sensitivity of CCs towards the 2%-doped ZnO NPs in co-culture experiments, during which the levels of oxidative stress were high enough to cause severe CC death, but not enough to affect the viability of NCs with lower metabolic rates. In contrast, pure ZnO NPs exhibited significant toxicity in both cancer and NCs, while 10%-doped NPs showed almost no effect in either of the cell types.

Other metals were also tested as potential dopants of ZnO NPs. For instance, in a study by Shakir *et al.* (2016), pure and different lanthanum-doped ZnO NPs (1%, 3% and 5% La/ZnO) were synthesized and their cytotoxicity was examined using various concentrations (6–500 μg mL^{-1}) in different CC lines, including MDA-MB-231, KCL22 (chronic myeloid leukemia) and HeLa cells.[164] Unlike Fe-doped NPs, La-doped ZnO NPs were

shown to be more potent at inducing cytotoxicity than pure ZnO NPs under the same experimental conditions. These findings suggest that in cases where specific cell types are resistant to ZnO NPs, doping them with La may enhance the NP dissolution kinetics and potentially serve as a means of enhancing toxicity. Recently, another study was conducted evaluating the cytotoxic effects of ZnO NPs doped with various lanthanides, including samarium (Sm), europium (Eu) and gadolinium (Gd).[165] They found that, in the Ehrlich ascites carcinoma (EAC) cell line, Sm^{3+} : ZnO displayed the most significant antitumor activity with 95% cell death, while both Eu^{3+} and Gd^{3+} caused only 10% and 5% tumor cell death, respectively. Pure ZnO NPs also showed weak antitumor activity, possibly due to the micro-sized particles utilized throughout the study. These findings are in line with the previously reported selective anticancer effects of nanocomplexes composed of Sm^{3+} and green tea polyphenols on the melanoma (B16F10) cell line.[166]

Finally, a study investigating the effects of varying NP surface modification was conducted using nano- and micro-particles of ZnO with sizes ranging from 40 nm to 1.2 μm.[167] These particles were either bare or coated with polyethylene glycol (PEG) or starch and were tested at various concentrations (1 μM to 7 mM). In human osteoblast CCs (MG-63), PEG-capped particles exerted higher toxicity with decreasing size and increasing concentration. In contrast, starch-capped ZnO exerted the lowest toxicity compared with the other particles, highlighting the importance of surface capping on ZnO toxicity towards CCs.

4.2.2. Metal-doped or coated CuO NPs. As with ZnO NPs, Fe-doping has been heavily investigated on CuO NPs with the aim of controlling the rapid release of Cu^{2+} from the particle surface. In a study by our group that was previously discussed in Section 3.1 wherein a model of the dissolution kinetics of Fe-doped CuO was developed based on solid-state diffusion, a homologous series of engineered CuO NPs was introduced with different levels of Fe-doping (1–10%) and tested in normal (BEAS-2B and murine MSCs) and cancerous cells (HeLa and KLN205).[79] In line with previous findings, there was a significant inverse correlation between Fe-doping and cell response in all tested cell types, including membrane damage, ROS production and cell death. The most significant anticancer activity was reported for the 6% Fe-doped CuO NPs at 12.5 μg mL^{-1}, which left NCs statistically unaffected. As previously mentioned, the dissolution profiles of these doped NPs were characterized by a two-step process, an initial fast burst-like release of Cu followed by a slow long-term release, with the total Cu^{2+} release from the 10% Fe-doped CuO NPs being 8%, in contrast with the ~65% observed in pure CuO NPs over a 10 minute time span. In a separate recent study comparing pure and 10% Fe-doped CuO NPs, results indicated similar intracellular Cu^{2+} accumulation and ROS generation for both NP types, although the doped NPs exhibited less redox activity and Cu^{2+} release as well as less severe loss in viability in C6 glioma cells.[168] Interestingly, the toxicity induced by both types of NPs was completely averted upon the co-administration of Cu chelators as well as the neutralization of lysosomal pH by bafilomycin A1.

Another type of metal-doping of CuO NPs was performed using Zn with the aim of inducing selective anticancer activity in glioma cells both *in vitro* and *in vivo* (Fig. 5).[169] Treatment with *n*Zn-doped CuO NPs has shown to not only inhibit cell proliferation in a DD manner, but also trigger ROS generation and the intrinsic apoptotic pathway. Specifically, it was found that *n*Zn–CuO NPs disturb cell growth by downregulating the gene expression of *bcl-2* and inhibiting AKT and ERK1/2. In a similar study, the anticancer activity of these particles was tested on human pancreatic CCs (AsPC-1 and MIA Paca-2).[170] Here, the authors highlight that the AMPK/mTOR pathway plays an important role in the inhibition of tumor growth induced by Zn–CuO NPs, as they increased both the protein levels and gene expression of p-AMPK, p-ULK1, Beclin-1 and the ratio of LC3-II/LC3-I, while NP exposure downregulated the phosphorylation of mTOR. The specificity of Zn–CuO NPs towards CCs was further tested in multiple cell lines.[171] In a DD manner, Zn–CuO NPs exerted anti-proliferative effects on CCs, including HepG2, Bel7402 (human hepatoma), A549, Panc28 (human pancreatic), HT1080 (human cervical), and Hela. However, in NC lines such as HUVEC and L02 (human hepatocyte) cells, these anti-proliferative effects were significantly weaker compared to the impact on CC lines. It was further shown that Zn–CuO NPs affect HepG2 and Panc28 CCs through ROS generation, apoptosis and the induction of G2/M cell cycle arrest. Molecular data revealed an increase in the expression of p-IKKα/β and nucleus p-NF-κB p65 and a decrease of IKKα, IKKβ, IκBα and nucleus NF-κB p65 expression in both HepG2 and Panc28 CC lines. In a parallel study that also revealed the importance of the NF-κB pathway, further treatment with NAC restored all of the above effects on protein expression.[172] Therefore, in addition to the activation of the AMPK/mTOR pathway, Zn–CuO NPs trigger the ROS-mediated NF-κB pathway during the selective inhibition of CC growth.

Besides metal doping, CuO NPs have been synthesized with a variety of coatings with the aim of controlling NP dissolution. Studer *et al.* (2010) reported that coating CuO NPs with a stabilizing carbon layer not only reduced their toxicity in CCs (HeLa) but also altered the release and cellular internalization of Cu^{2+}.[103] Protein coats have also been applied to CuO NPs to tune their toxicity towards C6 glioma cells, including dimercaptosuccinic acid (DMSA) and bovine serum albumin (BSA),[173] which are able to improve the colloidal stability of CuO NPs in physiological media.[174] Within these cells, DMSA protein-coated NPs (pCuO-NPs) resulted in Cu accumulation and severe toxicity in a time-, concentration- and temperature-dependent manner. Exposure of the cells to pCuO-NPs for 30 minutes caused severe loss in enzyme activity, including cellular lactate dehydrogenase (LDH) activity and MTT reduction capacity, which are markers for membrane integrity and cell viability, respectively. This effect was only detected in C6 glioma cells when the Cu content exceeded 20 nmol mg^{-1}. Once again, the addition of Cu chelators (TTM or BCS) led to lower intracellular Cu content and protected glioma cells against toxicity induced by pCuO-NPs.

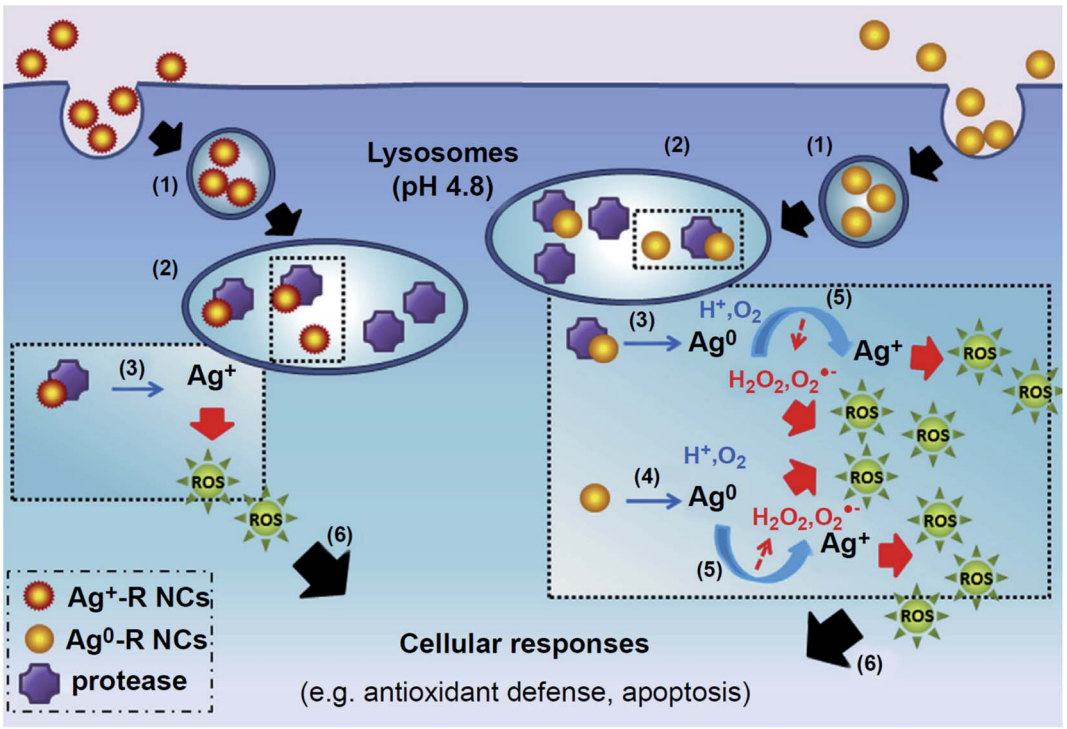

Fig. 5 Proposed mechanism of cellular responses induced by GSH-Ag NCs. GSH-Ag NCs were taken up by the cell *via* an endocytotic pathway (1) and send to the lysosome (2),where stable GSH-Agþ-R NCs were enzymatically degraded by the lysosomal protease (3) to form reactive Agþ. In contrast, GSH-Ag^0-R NCs decomposition originated not only from enzymatic degradation of the clusters (3) but also caused by their instability (4) in lysosome environment. The result of this decomposition is the formation of Ag^0, which then undergone oxidative dissolution (5), resulting in Ag^+ ion formation with ROS as the byproducts. Ag^+ ions being release in turn affects the cell's respiratory chain, leading to increase of ROS which then triggers cellular responses (6), such as activation of anti-oxidant defense and programmed cell death. Reproduced with permission from Setyawati *et al.*,[176] © 2014, Elsevier Publishing.

4.2.3. Coated Ag NPs. Despite the lack of studies on metal-doped Ag NPs, various efforts have been made to control Ag NP dissolution through varying surface coatings. In a study by Manshian *et al.* (2017), the cytotoxicity of citrate-coated Ag NPs was investigated by exposing various CC lines, such as HeLa, A549, and KLN205 to different NP concentrations for 24 h up to 5 days.[175] Using high-content imaging, they showed that these NPs induced toxicity through ROS generation, mitochondrial damage and autophagy, whereas the resulting immunomodulatory effects associated with NP treatment were characterized by an increase in the activity of the NFκB pathway and levels of the pro-inflammatory cytokine IL-1α in both HeLa and A549 cells under subcytotoxic conditions. PVP-coated Ag NPs were also tested for their toxicity on L5178Y-R murine lymphoma cells, which, at the maximum tested molar concentration of 57.9×10^{-8} M, were able to induce up to 78% cytotoxicity compared to the 100% toxicity caused by metal Ag at the same concentration.[97] Both formulations were also tested on normal murine thymic lymphocytes showing that PVP-coated Ag NPs induced proliferation at lower concentrations whereas toxicity was observed at higher concentrations. Metal Ag did not reveal any toxic effects for the tested conditions. This study indicated that PVP-coated Ag NPs and metal Ag induced cell death *via* a necrotic rather than apoptotic pathway.

In a separate study, the toxicity of Ag nanoclusters (Ag NCs) with two different core surface speciation (Ag^+-rich NCs (Ag^+-R NCs) and Ag^0-rich NCs (Ag^0-R NCs)) of the same size (<2 nm core) was investigated on human neonatal foreskin fibroblast cells (BJ).[176] Ag^0-R NCs induced higher cellular toxicity in a dose- and time-dependent manner, as well as higher ROS generation compared to the Ag^+-R NCs. As the Ag^0-R bond is weaker than Ag^+-R, making it more potent to release Ag in acidic environments, this difference in toxicity may be due to the faster release of Ag from Ag^0-R NCs which then oxidizes immediately to Ag^+ within the lysosomes. After 24 and 48 h of exposure to Ag^0-R NCs, only 47% and 15% of the viable population remained, respectively, while Ag^+-R NCs did not induce cell death in BJ cells. Activation of *p53* was increased by 3.3-fold by Ag^0-R NCs after 24 h, while only a 2-fold increase was observed for Ag^+-R NCs (Fig. 5).

Ag NPs embedded in microbial exopolysaccharides (EPS) and biogenerated by *Klebsiella oxytoca* DSM 29614 under aerobic (Ag NPs-EPS^{aer}) conditions were also investigated for their cytotoxic effects on SKBR3 cells.[177] Significant inhibition of cellular proliferation was observed, and the colony-forming ability, which was used to assess cell viability, showed a dose- and time-dependent reduction after Ag NPs-EPS^{aer} treatment. The selectivity of Ag NPs-EPS^{aer} for SKBR3 cells was confirmed by calculating the selectivity index using DOX as a positive

control and the non-tumoral mammary cell line HB2. Morphological assessment revealed apoptotic-like changes such as cell shrinkage, loss of contact between adjacent cells, membrane blebbing and nuclear chromatin condensation. Additionally, a concentration-dependent elevation of intracellular ROS was observed after 24 h of exposure. They found that autophagic cell death seemed to be the main mechanism in Ag NPs-EPS^{aer}-induced cell death within the first 24 h of treatment, as supported by the evaluation in the expression levels of multiple autophagic markers. Specifically, the upregulation of ATG5, ATG7, LC3-II and Beclin-1 and downregulation of AKT, p-AKT, p62 and HSP90 were detected. It was also shown that DNA was not a primary target within the first 24 h of treatment but in the long-term, treatment with Ag NPs-EPS^{aer} could increase and/or stabilise the interaction of Ag with DNA and thereby induce cell death. Together these results suggest that the cytotoxicity of Ag NPs-EPS^{aer} consists of a direct effect caused by cellular uptake and induction of intracellular ROS as well as an indirect effect caused by the release of Ag^+ – initially in the mitochondria and later on in the nuclei to interact with DNA – and is regulated by the induction of autophagy, followed by apoptosis.

Furthermore, Swanner *et al.* (2019) found that triple-negative breast cancer (TNBC) cells possess specific vulnerability to Ag NPs which can be exploited to avoid toxicity induction in normal tissue.[178] They found that internalization of the NPs is essential to exert any TNBC-selective cytotoxic effects and that selective inhibition of TNBC cell growth takes place regardless of NP size, shape or coating (including PVP). However, they show that TNBC cells and their normal counterparts are comparably sensitive to Ag^+, highlighting the importance of the NP itself in exerting a tumor selective response. Next, they followed the uptake and intracellular distribution of Ag NPs and reported that after 1 h of incubation with cells, Ag NPs were localized within the endosomes and exhibited clear degradation in MDA-MB-231 cells while remaining intact in non-malignant breast epithelial cells (MCF-10A). Interestingly, after 6 h, MCF-10A cells still displayed intact particles even upon endosomal fusion with lysosomes. The same observations were made when comparing the effects on iMEC and SUM159 cells, a non-malignant breast epithelial and TNBC cell line respectively. It was also shown that Ag NPs impaired the cellular redox balance in MDA-MB-231 cells and induced ER stress, UPR activation, and an increased expression of CHOP, a pro-apoptotic protein in TNBC cells. This effect was not observed in the MCF-10A cell line. Finally, MDA-MB-231 and non-neoplastic S1 mammary epithelial cells (S1 cells) were grown in 3D tumor organoid cultures, and in line with the previous findings, Ag NPs induced apoptosis and DNA damage only in MDA-MB-231 cells.

4.2.4. Coated IONPs. The degradation of IONPs has been clearly linked with the nature of the coating agent. Small molecules, such as citrate, have been shown to provide little protection against degradation, while polymeric coatings (dextran, or carboxydextran) were found to be slightly more stable.[61,179] When a lipid bilayer was attached directly onto the surface of the IONPs, this resulted in far more stable formulations. Also, silica and metal-based coatings (*e.g.* gold) have been shown to provide excellent stability against degradation.[180,181]

5. Cancer-specific NP toxicity *in vivo*: an overview of preclinical results obtained for NP degradation

Despite the multitude of *in vitro* studies that have been conducted over the years exploiting the M^{z+} release and ROS generation of ZnO, CuO and Ag NPs to selectively target CCs, only a few have made their way to the preclinical setting. Specifically, the lack of *in vivo* studies on pure ZnO and CuO NPs in the literature can be attributed to the high toxicity of these particles, which tend to cause major weight loss in animals and often premature death shortly after treatment. Thus, the termination of such experiments occurs due to the underlying ethical reasons associated with NP administration.[77] In this next section, we discuss the few *in vivo* experiments associated with pure ZnO, CuO, and Ag NP, as well as the progress that has been made over the recent years in rendering such studies safer *via* doping and coating of these NPs. A summary of all the discussed studies is provided in Tables 2–4.

5.1. Effects of pure ZnO, CuO, Ag and IONPs in mouse tumor models

Among the few studies that have tested the effects of ZnO NPs *in vivo*, El-Shorbagy (2019) administered ZnO NPs alone or in combination with 100 mg kg^{-1} body weight *N*-acetyl cysteine (NAC) – a GSH precursor that has shown to lower intracellular ROS levels[182,183] – to Ehrlich solid carcinoma (ESC)-bearing mice for a period of 7 days.[184] During the treatment, three different doses of ZnO NPs including 50, 300 and 500 mg kg^{-1} were administered through oral gavage. It was shown that treatment with NPs inhibited the tumor growth by 31.5% and 46% for the 300 and 500 mg kg^{-1} doses, respectively. In line with respective *in vitro* studies, a significant increase in *p53* and *bax* and a decrease in *bcl2* expression levels were observed along with significant reductions of glutathione-*S*-transferase (GST) and CAT. Their results suggest that ZnO NPs have a significant effect on the inhibition of tumor growth through induction of oxidative stress, DNA damage and activation of the *p53*-mediated pathway, leading to apoptosis. Additionally, pre-treatment with NAC was shown to protect normal tissue including the liver and kidney without interfering with the antitumor activity of the ZnO NPs. In the latest study, ZnO NPs were used to treat lung cancer in mice and were found to exert anticancer activity when a minimum dose of 0.25 mg kg^{-1} was administered.[185] However, contradicting results have been published by Hassan *et al.* (2017), wherein they observed an antioxidant effect of ZnO NPs, characterized by a decrease in rat serum α-fetoprotein (AFP) and α-L-fucosidase (AFU) levels and restoration of caspase-3 normal levels upon treatment of hepatocellular carcinoma (HCC)-bearing mice with ZnO NPs.[147] It must be noted that AFP and AFU have been shown to be common biomarkers of HCC tumors.[186]

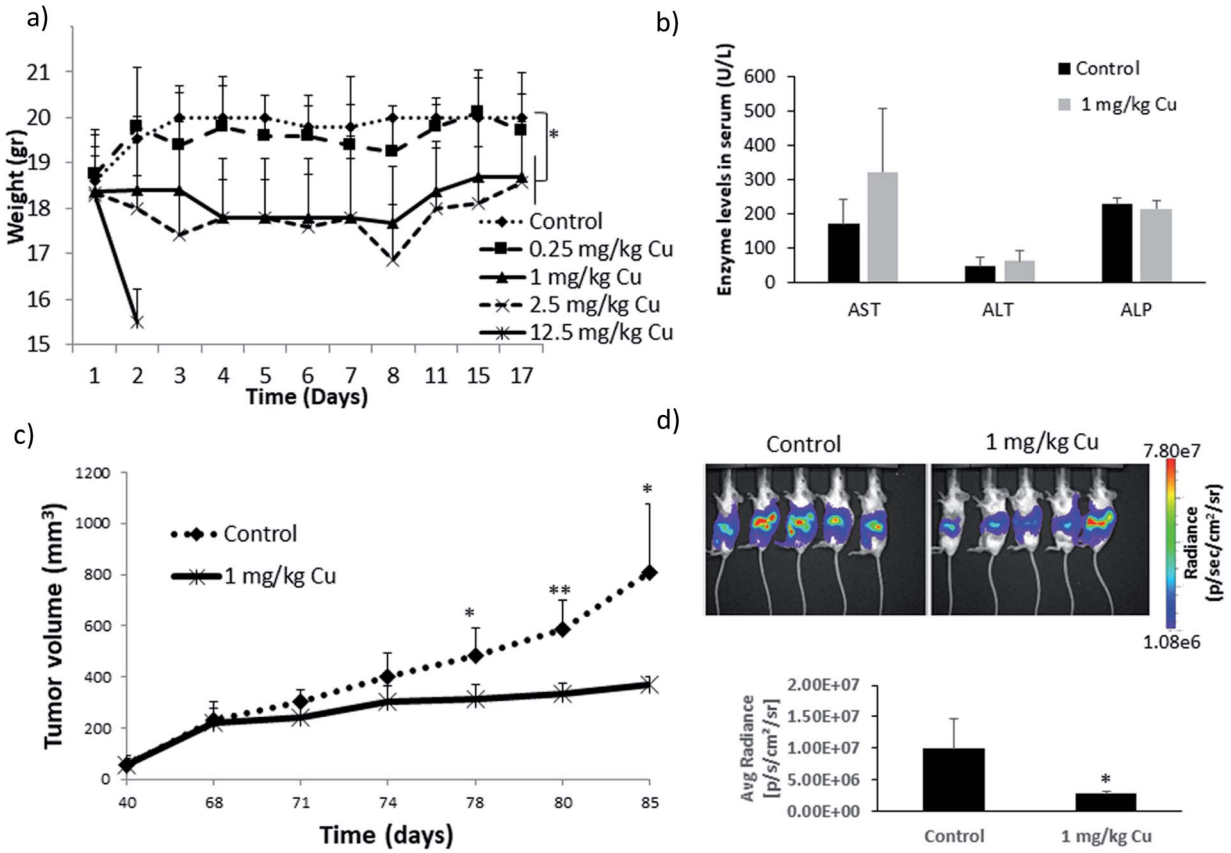

Fig. 6 *In vivo* studies of pure CuO NPs as reported by Benguigui *et al.*[149] (a) Effect of different doses of NPs on the weight of mice with no tumors over time. (b) Changes in the biomarkers of liver damage (AST, ALT, ALP) as a result of NP treatment in mice with no tumors. (c and d) Effect of daily CuO NP treatment (total 7 days) on tumor size in mice bearing subcutaneous PANC-1 tumors (c) and on the bioluminescence signal in orthotopically-implanted PANC-1 (luciferase-tagged) tumors after 5 weeks (d). Reproduced with permission from Benguigui *et al.*[149] © Nature Publishing Group, 2019.

The cytotoxic effects of pure CuO NPs have been investigated in mice bearing pancreatic tumors (Fig. 6) and were shown to delay tumor growth and significantly increase the number of apoptotic TICs, which is in line with previously discussed *in vitro* studies.[149]

With respect to Ag NPs, their effect on the progression and growth of human lung CCs (H1299) has been evaluated in immunodeficient SCID mice.[152] The Ag NPs which were administered intraperitoneally were able to slow down the development of tumors and significantly reduce their size. Another study assessed the antitumor activity of pure Ag NPs in EAC-bearing mice and showed that a dose of 5 mg kg^{-1} could significantly inhibit the cell volume, cell count and weight of the tumors, as compared to the non-treated control group.[153] A rapid increase in ascitic tumor volume and a decrease in body weight was observed in the control and treated mice, respectively. The body weight was correlated with the ascites fluid volume, which served as a direct nutritional source for tumor cells. These results are in agreement with a previous report on an Ehrlich ascites tumor model in mice, in which the antitumor activity of biologically synthetized Ag NPs was detected.[155] In this study, increases in nitric oxide, MDA and ROS levels, and DNA damage were reported, and were associated with higher numbers of necrotic and apoptotic cells as shown on photomicrographs of H&E sections. Histopathological observations and cell cycle analysis also revealed an antiangiogenic effect of Ag NPs. In another similar study that employs biologically-synthesized particles, *Ficus religiosa*-derived Ag NPs were examined for their anticancer activity in a mouse model of Dalton's ascites lymphoma (DAL).[187] As was the case in the previous study, NP-treated mice experienced loss of body weight (in line with reduced ascites fluid volume) as well as increased survival. These Ag NPs were shown to induce CC apoptosis *via* DNA damage and exert antioxidant (restoration of MDA, SOD and CAT levels) and antiangiogenic effects without affecting kidney and liver function.

For IONPs, no cancer-selective toxicity has been observed, but clinically approved dextran-coated IONPs have been shown to activate macrophages to a pro-inflammatory M1-type status. This then further resulted in a reduction in the growth of subcutaneous adenocarcinoma, due to a more aggressive immune microenvironment.[188] This indirect effect could play an important role in macrophage-related cancer immunotherapies.

5.2. *In vivo* effects of doped and coated NPs

5.2.1. Metal-doped ZnO NPs. To enhance the anticancer selectivity and circumvent the major drawbacks associated with

the *in vivo* administration of ZnO NPs, including rapid weight loss and animal death shortly after NP treatment, the promising results of doped ZnO NPs in the *in vitro* settings were followed by preclinical *in vivo* experiments using mouse models. In one of these studies, the effects of pure, 2% and 10% Fe-doped ZnO NPs were tested and compared in DBA/2 mice bearing firefly luciferase-expressing KLN205 tumors.[77] When the tumor size reached a certain threshold (50 mm^3), NPs were administered peritumorally, and after 24 h, the release of free Zn^{2+} was quantified by means of a fluorescent signal. In agreement with their *in vitro* results, the levels of Zn^{2+} had a negative correlation with the degree of Fe-doping. When testing the therapeutic efficacy of pure ZnO NPs, these particles showed signs of toxicity at levels that caused the premature deaths of several mice. However, for the 2% and 10% Fe-doped ZnO NPs there were no clear signs of toxicity on the general health of the mice, and the therapeutic effect only became significant after 10 days. For the 10%-doped treated animals, the tumor growth was delayed in comparison to the control group, while the 2% Fe-doped ZnO NPs exhibited more effective results, with near-steady tumor sizes lasting at least 5 weeks. However, under the employed conditions, no complete destruction of the tumor could be obtained, although the peritumoral administration of the Fe-doped ZnO NPs resulted in a clear decrease in the number of metastases. Therefore, the preclinical evaluation of the Fe-doped ZnO NPs indicated a localized increase in free Zn^{2+} within the CCs that not only obstructed tumor growth, but also reduced the formation of metastases.

Another recent work in 2020 was carried out in which Sm-doped ZnO NPs were tested in Swiss albino female mice after the LD_{50} was determined.[165] The selected dose was 45 mg kg^{-1} (20% of LD_{50}) given that it exhibited no mortality and was administered by intramuscular injection to the Ehrlich solid tumor-bearing mice. While the average tumor size in the control group increased over time, the treated mice experienced reduced tumor size and a downregulation in CXCR4 and cytochrome P450 expression, which are markers of different aspects of cancer.[189,190]

5.2.2. Metal-doped CuO NPs. Doped CuO NPs have also been investigated *in vivo*, and a recent study by our team demonstrates the effects of Fe-doping on CuO NPs in syngeneic subcutaneous mouse models (KLN205 and CT26).[79] The percentage of Fe-doping was first optimized in several *in vitro* studies previously mentioned in Section 4.2.2, which consequently uncovered the 6% Fe-doped CuO NPs as the optimal formulation. While the effects of pure and 6% Fe-doped CuO NPs on tumor growth were comparable, the un-doped particles negatively affected the body weight, resulting in the premature death of some mice. Next, we tested the combination therapy of 6% Fe-doped CuO NPs and epacadostat (EPAC), a strong inhibitor of IDO1 immunosuppression, which showed increased therapeutic efficacy and complete tumor remission, compared to animals receiving a combined therapy of DOX and EPAC. Moreover, tumor cell rechallenge (*via* repeated vaccinations after complete remission) prevented tumor growth, and relapse was absent for up to 6 months. Additionally, no metastasis was observed throughout the experiment. While NPs alone resulted in the inhibition of cancer growth, a total remission was only achieved when combined with an immunosuppression inhibitor (Fig. 7). NP-induced sensitization of the immune system seemed to be regulated by NLRP3 inflammasome activation, combined with the immunogenic character of the CC-death mechanism. Evidence of a local anti-tumor immune response was shown by an increased influx of immune cells and activation of cytotoxic (CD8+) T cells and natural killer cells in CT26 tumors of BALB/c mice after combined treatment with 6% Fe-doped CuO NPs and EPAC. Together these results demonstrate that the gradual long-term release of Cu^{2+} due to NP-mediated degradation, combined with elevated ROS generation, exerts a vaccination-like effect for anti-cancer immune activation.

At the same time, the potential of Zn-doped CuO nanocomposites to selectively target CCs has been investigated in multiple studies *in vivo*. In a glioblastoma mouse model established by U87 cell transplantation, significant antitumor effects of Zn–CuO NPs have been demonstrated.[169] Specifically, increased procaspase-9 and procaspase-3 levels and a decreased BCL2/BAX ratio indicated that NP-mediated cell death occurs through the mitochondrial apoptotic pathway. Histological studies confirmed a DD decrease in Ki-67, a marker for cell proliferation, as well as no toxicity in the main organs. Furthermore, this study demonstrated that temozolomide (TMZ)-resistance of cells can be reversed upon Zn–CuO NP exposure *via* inhibition of AKT/ERK1/2 activation. Similar observations on tumor growth inhibition have been made in mice bearing pancreatic cancer tumors (Panc28 (ref. 172) and AsPC-1 (ref. 170)) upon treatment with Zn–CuO NPs.

5.2.3. Coated Ag NPs. In an early study by Liu *et al.* (2012), cell-penetrating peptides (CPP-TAT) were functionalized on the surfaces of Ag NPs with the aim of enhancing the cellular uptake of the NPs.[191] In contrast to the typical method of NP internalization *via* endocytosis, CPPs are able to directly transport NPs across cellular membranes and immediately gain cytosolic rather than endosomal access. This strategy was used for the treatment of multidrug-resistant (MDR) cancer and was compared with non-functionalized 8 nm Ag NPs. These TAT-Ag NPs did not only exhibit strong anticancer activity *in vitro*, but also significantly inhibited tumor growth in mice with malignant melanoma at a lower dose (1 nmol kg^{-1}) than the effective dose of DOX (4.3 μmol kg^{-1}). Although both groups of mice showed similar results with respect to tumor growth, DOX-treated mice were associated with significant weight loss, whereas mice treated with Ag NPs or AgNP-TAT gained weight throughout the therapy. PVP-coated Ag NPs were also evaluated for their antitumor activity in a L5178Y-R murine lymphoma cell mouse model and compared with metal Ag and vincristine, a common chemotherapeutic.[97] Results showed that treatment with PVP-coated Ag NPs or metal Ag, at a dose of 20 mg kg^{-1} and given at the time of tumor inoculation *via* intramuscular injection, significantly increased the survival response compared to the following groups: (a) same treatments administered 7 days after tumor injection, (b) treatment with vincristine, and (c) the untreated L5178Y-R tumor-bearing mice. Survival rates at day 35 were reported as 60%, 70%, 25%, 55%,

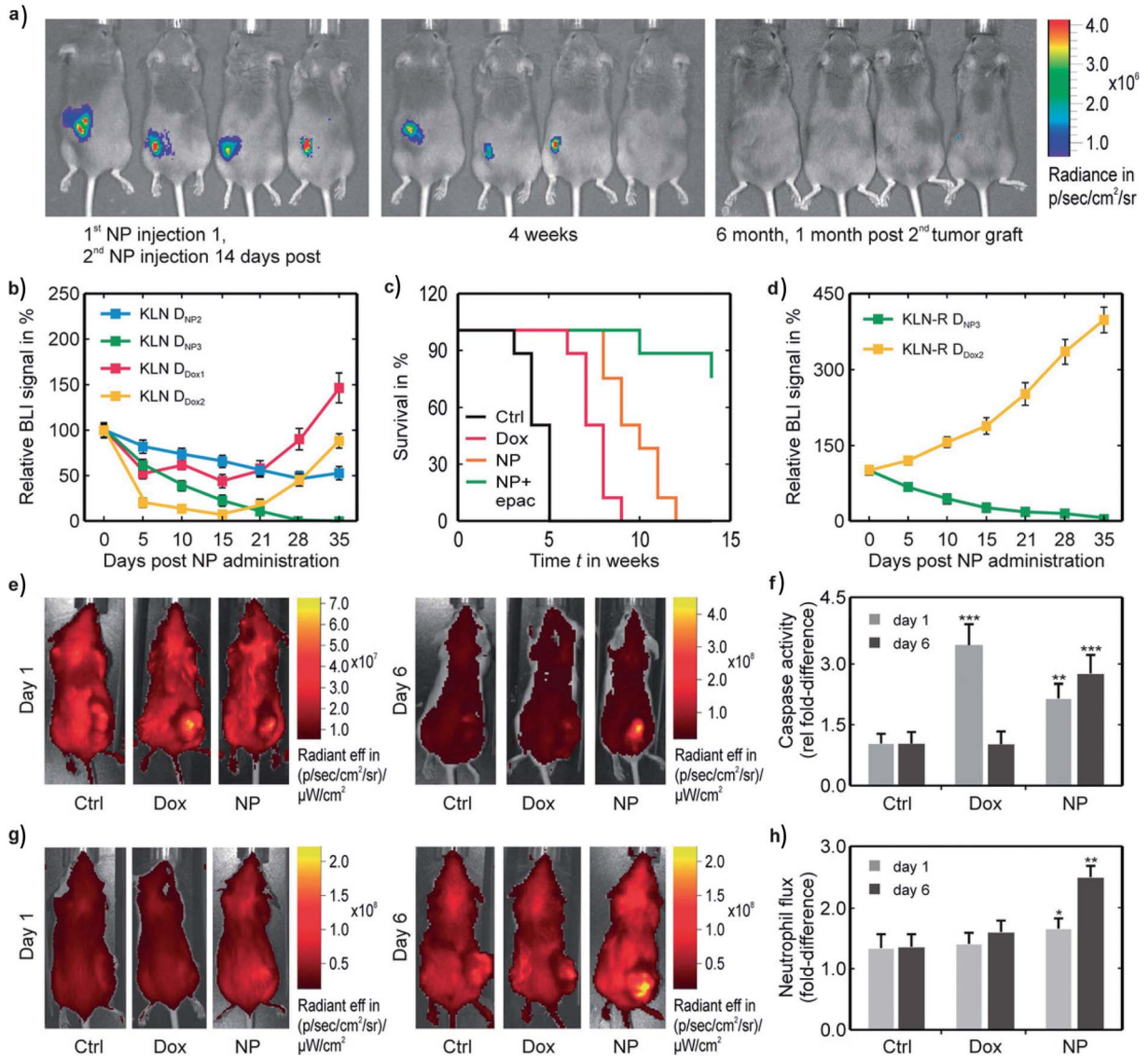

Fig. 7 Synergistic therapeutic effect of treatment combinations with 6% Fe-doped CuO NPs and EPAC in mice bearing firefly-expressing KLN205 (a–d) or CT26 (e–h) tumors, as assessed by Naatz *et al.*[79] (a) Luminescence images of tumors after treatment over time. (b and d) Bioluminescence imaging (BLI) signals comparing combination treatments of EPAC with either NPs or DOX in normal (b) and DOX-resistant cells (d). (c) Survival curves of mice exposed to different treatments. (e–h) Fluorescence images of mice treated with a fluorescent pan-caspase probe (e) and neutrophil-specific peptide (g) and their respective signal quantifications. The DOX and NP-treated groups also received EPAC. This image has been reproduced with permission from Naatz *et al.*,[79] © Wiley-VCH, 2020.

50% and 20% for the various groups respectively. Furthermore, PVP-coated Ag NPs were tested on a TNBC mouse xenograft model and were shown to reduce the tumor growth rate compared the control group.[178] All the NP-treated animals survived beyond the experimental period (100 days), in contrast to the one third survival rate experienced by the control group.

To investigate the contribution of the immune system to the effects of citrate-coated Ag NPs on the treatment of cancer, Manshian *et al.* (2017) administered Ag NPs to immune-deficient as well as immune-competent mice bearing KLN 205 CCs.[175] In a first experiment, the pro-inflammatory effects of the Ag NPs were tested. The relative fluorescence intensity – originating from an inflammation-activatable probe given to the animals 5 days post saline or NP administration – exhibited a higher signal in the NP-treated immune-competent mice, indicating tumor inflammation and thus activation of the immune system. In a parallel experiment using the same animal groups, the therapeutic efficacy of the NPs was evaluated, during which a clear reduction in tumor size was shown upon NP treatment. Ten days post treatment, tumors regrew due to the dilution of cellular NP levels that results from continuous cell division. At the same time, for the treated immune-deficient mice, the tumor growth rate was nearly identical to that observed in the untreated group, highlighting the importance of the complementary role of the immune system during Ag NP cancer treatment.

6. Hypothetical mechanism summary

While all the NPs described above have redox potential and can induce ROS while undergoing degradation in the endo- or lysosomal environment, the true mechanism behind cancer-selective toxicity remains somewhat unclear, and the lack of effect for IONPs compared to other NPs also remains unanswered. From our perspective, and based on the literature review, we suggest a hypothetical mechanism for both activities.

First, the ability of CuO, ZnO or Ag NPs to induce cancer cell selective toxicity may be due to the fact that many cancer cells have a high metabolic rate and intrinsically have higher levels of (mitochondrial) ROS. Any additional ROS that is generated, such as that generated by the NPs, can therefore result in exaggerated toxic effects compared to non-cancerous counterparts. For every cell, cellular defense mechanisms against ROS will protect the cell against certain levels of ROS generation.[192] However, when this threshold is exceeded, oxidative stress occurs, which can be lethal to the cells. It is therefore important to finely tune the kinetics of NP degradation and associated ROS generation to be able to induce sufficient ROS to exceed toxic limits in cancerous cells, while not inducing too many that they would also affect non-cancerous cells. Furthermore, the effects observed may not be generalized to every type of cancerous or normal cell. If the cancer cells have a high level of oxidative defense mechanisms, then they will not be easily targeted by this form of therapy. Cancer cells that contain mutations that limit their oxidative stress defenses would however be excellently suited to this type of therapy.

Secondly, the ability of some NPs to induce cancer-selective toxicity while others cannot (*e.g.* IONP), can simply be due to the chemical nature of the metal ion and how these are normally processed under typical physiological conditions. For Fe, any Fe to be taken up by cells will be bound to transferrin, and cellular uptake involves the transferrin molecule binding to the cell surface-located transferrin receptor. This triggers an internalization pathway, where the transferrin receptor/transferrin complex is shuttled inside early endosomes and at lower pH, Fe is released. The transferrin receptor can then be recycled back to the cell membrane, while Fe can be transferred to late endosomes or lysosomes. It can then bind to small molecules, such as citrate, which can shuttle it into the cytoplasm, where it can become part of the labile Fe pool.[193] When cellular Fe levels increase, they can be stored long-term in Fe storage proteins (ferritin), the level of which depends on the amount of cytoplasmic Fe. For IONPs, this would essentially be a similar story, where internalization of IONPs results in endo- or lysosomal sequestration of the NPs followed by their degradation and transport of free Fe ions by means of citrate to become part of the labile Fe pool.[160] Excessive amounts of Fe can be relatively well tolerated by increasing the level of ferritin storage complexes. Any toxicity would be linked to excessive amounts of Fe in the endo- or lysosomes, linked to high levels of Fenton reactions that exceed local toxicity thresholds.

For Ag, Zn or Cu, the physiological handling of these ions is far different. For Ag, which is extremely rare in our body, there are no specific transport pathways or predetermined routes of cellular processing. Ag ions will mainly be linked to calcium channels, and monovalent metal transporters.[194] For Zn ions, a highly specific pathway is present. In short, for eukaryotic cells, Zn ions are transported from the extracellular space into the cell cytoplasm by the so-called Zrt-, Irt-like protein (ZIP, SLC39) while the cation diffusion facilitator (CDF, SLC30) work the opposite way and transport Zn from the cytoplasm to the extracellular space. Once inside the cytoplasm, Zn can be transported to the Golgi apparatus, or mitochondria, where it can be used in Zn-dependent proteins or matrices.[195] For Cu, the process is similar. Here, Cu enters the cells mainly *via* the Cu transporter 1 (CTR1), and is immediately linked to its chaperones, such as Cu chaperone for SOD (CCS) or an enzyme involved in the synthesis of cytochrome c oxidase (Sco1).[196] Cu can be then stored at low levels in MTs. For Ag, Zn or Cu, it is therefore important to note that transport of these ions from endo- and lysosomes towards the cytoplasm is very limited as it does not occur naturally. For metal-containing NPs, this thus poses an entirely different scenario, where the cell is not naturally equipped to deal with excess level of the M^{z+} in its endosomal compartments. ZnO, CuO or Ag NP, all of which typically dissolve rather quickly, result in free M^{z+} already present in cell medium due to premature degradation, and cellular uptake of excess M^{z+} that can lead to cell death.[197] Alternatively, leakage of M^{z+} from endosomes can also lead to further oxidative stress and cytotoxicity, while the intraendosomal presence of these M^{z+} in itself can generate additional ROS.

7. Conclusion and future outlook

Here, we have summarized recent advances and key mechanisms behind the degradation of degradable metal and MO NPs. We highlight the various types of doping strategies and surface coatings that have been used to control NP dissolution and achieve selective tumor targeting, as well as certain computational models that have been developed to predict the impact of various physicochemical alterations on cytotoxicity. Besides the composition of the surface modifications, the toxicity profiles of these NPs have been optimized by changing the size, aspect ratio, and concentration of dopants and surface coatings. We then discussed several recent *in vitro* and *in vivo* advances that utilized these variously modified NPs to highlight their great potential in selective cancer therapy.

Studies assessing the toxicity of pure ZnO, CuO and Ag NPs on a wide variety of cell lines showed a dose-dependent toxicity, as well as a time-dependent mechanism. In addition, cellular studies on Fe- and lanthanide-doped ZnO NPs showed the potential fine-tuning capacities of the doping approach to control their cytotoxicity. Similar results were found for carbon-coated, protein-coated and Fe-doped CuO NPs, and for citrate- and EPS-coated Ag NPs. At the same time, pure ZnO, CuO and Ag NPs have not been extensively investigated *in vivo*, due to their high cytotoxicity levels that cause premature death in animals shortly after treatment. Nevertheless, *in vivo* research on their coated and doped counterparts have gained tremendous interest over the recent years, although the NPs remain in

the early phases of development. Specifically, doping of ZnO NPs with Fe and samarium, as well as coating Ag with citrate for instance, have provided a first glimpse of the potential use of these particles in cancer therapy. For CuO NPs, doping with Fe and Zn have exhibited promising results *in vivo*, especially in combination with epacadostat, which achieved complete tumor remission.[79]

Therefore, the latest advances on controlling NP dissolution provide a positive outlook in the direction of selective tumor targeting, indicating a promising future for the use of nanotechnology in cancer therapy. Still, several aspects require further investigation to improve the clinical translation of such NMs, including the inconsistencies in *in vitro* research concerning the setup, NP synthesis methods and evaluated parameters, making it hard to reproducibly come to the same results in follow-up studies. In particular, a GMP-certified synthesis method that can produce the levels of NPs required for clinical use is essential and more work is needed to set up such GMP-certified synthesis methods. Another aspect involves a further understanding of their underlying biological pathways. Several studies already suggest mechanisms and pathways involved in NP-induced cancer cell death, yet more understanding is needed to make firm conclusions. This in particular addresses the reason why some cancer cell types are more sensitive to this type of NP-mediated therapy than others, irrespective of the NP internalization levels. If any biomarkers could be found that can predict whether a particular tumor type would be sensitive to this of treatment or not would be a major breakthrough. Another point of attention would be the ability of the NPs to induce immunogenic cell death and hereby sensitize the tumors to immunotherapy. A broader spectrum of studies must be performed to understand whether this is true for all NPs or which NP-related parameters can enhance this. Additionally, also here the question of tumor-type specificity comes up, where the biological outcome of NP treatment will likely also depend on the nature of the tumor cells and its immune microenvironment. Lastly, while some promising preclinical studies have been performed, this must be repeated on a broader range of tumor types, and also include more relevant tumor models, such as patient-derived xenografts, and by combining different immunotherapy-NP combinations in view of the tumoral immune landscape.

Conflicts of interest

There are no conflicts to declare.

References

1 *Lancet*, 2003, **362**, 673.
2 S. C. Baetke, T. Lammers and F. Kiessling, *Br. J. Radiol.*, 2015, **88**, 20150207.
3 V. Wagner, A. Dullaart, A.-K. Bock and A. Zweck, *Nat. Biotechnol.*, 2006, **24**, 1211–1217.
4 A. Nel, T. Xia, L. Mädler and N. Li, *Science*, 2006, **311**, 622–627.
5 L. E. Euliss, J. A. DuPont, S. Gratton and J. DeSimone, *Chem. Soc. Rev.*, 2006, **35**, 1095–1104.
6 V. P. Chauhan and R. K. Jain, *Nat. Mater.*, 2013, **12**, 958.
7 A. C. Anselmo and S. Mitragotri, *Bioeng. Transl. Med.*, 2019, **4**, e10143.
8 C. Buzea, I. I. Pacheco and K. Robbie, *Biointerphases*, 2007, **2**, MR17–MR71.
9 C. Sioutas, R. J. Delfino and M. Singh, *Environ. Health Perspect.*, 2005, **113**, 947–955.
10 G. Oberdörster, A. Maynard, K. Donaldson, V. Castranova, J. Fitzpatrick, K. Ausman, J. Carter, B. Karn, W. Kreyling and D. Lai, *Part. Fibre Toxicol.*, 2005, **2**, 8.
11 Y. Wei, L. Quan, C. Zhou and Q. Zhan, *Nanomedicine*, 2018, **13**, 1495–1512.
12 S. K. Golombek, J.-N. May, B. Theek, L. Appold, N. Drude, F. Kiessling and T. Lammers, *Adv. Drug Delivery Rev.*, 2018, **130**, 17–38.
13 H. Maeda, G. Bharate and J. Daruwalla, *Eur. J. Pharm. Biopharm.*, 2009, **71**, 409–419.
14 H. L. Karlsson, J. Gustafsson, P. Cronholm and L. Möller, *Toxicol. Lett.*, 2009, **188**, 112–118.
15 C. Maksoudian, S. J. Soenen, K. Susumu, E. Oh, I. L. Medintz and B. B. Manshian, *Bioconjugate Chem.*, 2020, **31**, 1077–1087.
16 M. J. Akhtar, M. Ahamed and H. A. Alhadlaq, *Clin. Chim. Acta*, 2018, **487**, 186–196.
17 S. Fraga, A. Brandão, M. E. Soares, T. Morais, J. A. Duarte, L. Pereira, L. Soares, C. Neves, E. Pereira and M. de Lourdes Bastos, *Nanomedicine*, 2014, **10**, 1757–1766.
18 J.-Y. Wang, J. Chen, J. Yang, H. Wang, X. Shen, Y.-M. Sun, M. Guo and X.-D. Zhang, *Int. J. Nanomed.*, 2016, **11**, 3475.
19 W. Poon, Y.-N. Zhang, B. Ouyang, B. R. Kingston, J. L. Wu, S. Wilhelm and W. C. Chan, *ACS Nano*, 2019, **13**, 5785–5798.
20 S. Sabella, R. P. Carney, V. Brunetti, M. A. Malvindi, N. Al-Juffali, G. Vecchio, S. M. Janes, O. M. Bakr, R. Cingolani and F. Stellacci, *Nanoscale*, 2014, **6**, 7052–7061.
21 K. Midander, P. Cronholm, H. L. Karlsson, K. Elihn, L. Möller, C. Leygraf and I. O. Wallinder, *Small*, 2009, **5**, 389–399.
22 R. a. Weissleder, D. D. Stark, B. L. Engelstad, B. R. Bacon, C. C. Compton, D. L. White, P. Jacobs and J. Lewis, *Am. J. Roentgenol.*, 1989, **152**, 167–173.
23 F. Danhier, E. Ansorena, J. M. Silva, R. Coco, A. Le Breton and V. Préat, *J. Controlled Release*, 2012, **161**, 505–522.
24 A. Abdal Dayem, M. K. Hossain, S. B. Lee, K. Kim, S. K. Saha, G.-M. Yang, H. Y. Choi and S.-G. Cho, *Int. J. Mol. Sci.*, 2017, **18**, 120.
25 O. Augusto and S. Miyamoto, *Principles of free radical biomedicine*, 2011, vol. 1, pp. 19–42.
26 B. Halliwell, *Plant Physiol.*, 2006, **141**, 312–322.
27 C. F. Mueller, K. Laude, J. S. McNally and D. G. Harrison, *Arterioscler., Thromb., Vasc. Biol.*, 2005, **25**, 274–278.
28 M. J. Akhtar, M. Ahamed, H. A. Alhadlaq and A. Alshamsan, *Biochim. Biophys. Acta, Gen. Subj.*, 2017, **1861**, 802–813.
29 Y. R. Li, *Free Radical Biomedicine: Principles, Clinical Correlations, and Methodologies*, Bentham Science Publishers, 2012.

30 V. J. Thannickal and B. L. Fanburg, *Am. J. Physiol.: Lung Cell. Mol. Physiol.*, 2000, **279**, L1005–L1028.
31 M. J. Akhtar, M. Ahamed and H. A. Alhadlaq, *Clin. Chim. Acta*, 2017, **469**, 53–62.
32 T. Finkel, *J. Biol. Chem.*, 2012, **287**, 4434–4440.
33 P. S. Brookes, Y. Yoon, J. L. Robotham, M. Anders and S.-S. Sheu, *Am. J. Physiol.: Cell Physiol.*, 2004, **287**, C817–C833.
34 C. Tapeinos and A. Pandit, *Adv. Mater.*, 2016, **28**, 5553–5585.
35 T. Xia, M. Kovochich, M. Liong, L. Madler, B. Gilbert, H. Shi, J. I. Yeh, J. I. Zink and A. E. Nel, *ACS Nano*, 2008, **2**, 2121–2134.
36 P. D. Ray, B.-W. Huang and Y. Tsuji, *Cell. Signalling*, 2012, **24**, 981–990.
37 T. Xia, M. Kovochich, J. Brant, M. Hotze, J. Sempf, T. Oberley, C. Sioutas, J. I. Yeh, M. R. Wiesner and A. E. Nel, *Nano Lett.*, 2006, **6**, 1794–1807.
38 G. G. Xiao, M. Wang, N. Li, J. A. Loo and A. E. Nel, *J. Biol. Chem.*, 2003, **278**, 50781–50790.
39 P. Talalay, A. T. Dinkova-Kostova and W. D. Holtzclaw, *Adv. Enzyme Regul.*, 2003, **43**, 121–134.
40 I. M. Kennedy, D. Wilson and A. I. Barakat, *Research report*, Health Effects Institute, 2009, pp. 3–32.
41 Z. Zhang, A. Berg, H. Levanon, R. W. Fessenden and D. Meisel, *J. Am. Chem. Soc.*, 2003, **125**, 7959–7963.
42 S. Pokhrel, A. E. Nel and L. Mädler, *Acc. Chem. Res.*, 2013, **46**, 632–641.
43 H.-M. Lee, D.-M. Shin, H.-M. Song, J.-M. Yuk, Z.-W. Lee, S.-H. Lee, S. M. Hwang, J.-M. Kim, C.-S. Lee and E.-K. Jo, *Toxicol. Appl. Pharmacol.*, 2009, **238**, 160–169.
44 H. Fenton, *J. Chem. Soc., Trans.*, 1894, **65**, 899–910.
45 Y. Wei and M. Guo, *Angew. Chem., Int. Ed.*, 2007, **46**, 4722–4725.
46 B. M. Strauch, R. K. Niemand, N. L. Winkelbeiner and A. Hartwig, *Part. Fibre Toxicol.*, 2017, **14**, 28.
47 H. Líbalová, P. M. Costa, M. Olsson, L. Farcal, S. Ortelli, M. Blosi, J. Topinka, A. L. Costa and B. Fadeel, *Chemosphere*, 2018, **196**, 482–493.
48 N. M. Franklin, N. J. Rogers, S. C. Apte, G. E. Batley, G. E. Gadd and P. S. Casey, *Environ. Sci. Technol.*, 2007, **41**, 8484–8490.
49 C. Beer, R. Foldbjerg, Y. Hayashi, D. S. Sutherland and H. Autrup, *Toxicol. Lett.*, 2012, **208**, 286–292.
50 P. Cronholm, H. L. Karlsson, J. Hedberg, T. A. Lowe, L. Winnberg, K. Elihn, I. O. Wallinder and L. Möller, *Small*, 2013, **9**, 970–982.
51 A. R. Gliga, S. Skoglund, I. O. Wallinder, B. Fadeel and H. L. Karlsson, *Part. Fibre Toxicol.*, 2014, **11**, 11.
52 M. Heinlaan, A. Ivask, I. Blinova, H.-C. Dubourguier and A. Kahru, *Chemosphere*, 2008, **71**, 1308–1316.
53 N. M. Franklin, N. J. Rogers, S. C. Apte, G. E. Batley, G. E. Gadd and P. S. Casey, *Environ. Sci. Technol.*, 2007, **41**, 8484–8490.
54 S. W. Wong, P. T. Leung, A. Djurišić and K. M. Leung, *Anal. Bioanal. Chem.*, 2010, **396**, 609–618.
55 T. W. Turney, M. B. Duriska, V. Jayaratne, A. Elbaz, S. J. O'Keefe, A. S. Hastings, T. J. Piva, P. F. Wright and B. N. Feltis, *Chem. Res. Toxicol.*, 2012, **25**, 2057–2066.
56 A. Ivask, K. G. Scheckel, P. Kapruwan, V. Stone, H. Yin, N. H. Voelcker and E. Lombi, *Nanotoxicology*, 2017, **11**, 150–156.
57 J. Llop, I. Estrela-Lopis, R. F. Ziolo, A. González, J. Fleddermann, M. Dorn, V. G. Vallejo, R. Simon-Vazquez, E. Donath and Z. Mao, *Part. Part. Syst. Charact.*, 2014, **31**, 24–35.
58 S. K. Misra, S. Nuseibeh, A. Dybowska, D. Berhanu, T. D. Tetley and E. Valsami-Jones, *Nanotoxicology*, 2014, **8**, 422–432.
59 A. L. Neal, N. Kabengi, A. Grider and P. M. Bertsch, *Nanotoxicology*, 2012, **6**, 371–380.
60 P. Asharani, M. P. Hande and S. Valiyaveettil, *BMC Cell Biol.*, 2009, **10**, 65.
61 S. J. Soenen, U. Himmelreich, N. Nuytten, T. R. Pisanic, A. Ferrari and M. De Cuyper, *Small*, 2010, **6**, 2136–2145.
62 S. Kim, J. E. Choi, J. Choi, K.-H. Chung, K. Park, J. Yi and D.-Y. Ryu, *Toxicol. In Vitro*, 2009, **23**, 1076–1084.
63 E. M. Luther, M. M. Schmidt, J. Diendorf, M. Epple and R. Dringen, *Neurochem. Res.*, 2012, **37**, 1639–1648.
64 T. S. Peretyazhko, Q. Zhang and V. L. Colvin, *Environ. Sci. Technol.*, 2014, **48**, 11954–11961.
65 J. Liu and R. H. Hurt, *Environ. Sci. Technol.*, 2010, **44**, 2169–2175.
66 R. Ma, C. Levard, S. M. Marinakos, Y. Cheng, J. Liu, F. M. Michel, G. E. Brown Jr and G. V. Lowry, *Environ. Sci. Technol.*, 2012, **46**, 752–759.
67 K. Kawata, M. Osawa and S. Okabe, *Environ. Sci. Technol.*, 2009, **43**, 6046–6051.
68 J. Fabrega, S. R. Fawcett, J. C. Renshaw and J. R. Lead, *Environ. Sci. Technol.*, 2009, **43**, 7285–7290.
69 H.-J. Eom and J. Choi, *Environ. Sci. Technol.*, 2010, **44**, 8337–8342.
70 V. Frazzini, E. Rockabrand, E. Mocchegiani and S. Sensi, *Biogerontology*, 2006, **7**, 307–314.
71 J. M. Falcón-Pérez and E. C. Dell'Angelica, *Exp. Cell Res.*, 2007, **313**, 1473–1483.
72 A. Okado-Matsumoto and I. Fridovich, *J. Biol. Chem.*, 2001, **276**, 38388–38393.
73 I. G. Gazaryan, I. P. Krasinskaya, B. S. Kristal and A. M. Brown, *J. Biol. Chem.*, 2007, **282**, 24373–24380.
74 A. M. Brown, B. S. Kristal, M. S. Effron, A. I. Shestopalov, P. A. Ullucci, K.-F. R. Sheu, J. P. Blass and A. J. Cooper, *J. Biol. Chem.*, 2000, **275**, 13441–13447.
75 S. L. Sensi, H. Z. Yin, S. G. Carriedo, S. S. Rao and J. H. Weiss, *Proc. Natl. Acad. Sci. U. S. A.*, 1999, **96**, 2414–2419.
76 K. E. Dineley, T. V. Votyakova and I. J. Reynolds, *J. Neurochem.*, 2003, **85**, 563–570.
77 B. B. Manshian, S. Pokhrel, U. Himmelreich, K. Tämm, L. Sikk, A. Fernández, R. Rallo, T. Tamm, L. Mädler and S. J. Soenen, *Adv. Healthcare Mater.*, 2017, **6**, 1601379.
78 D. Denoyer, S. Masaldan, S. La Fontaine and M. A. Cater, *Metallomics*, 2015, **7**, 1459–1476.
79 H. Naatz, B. B. Manshian, C. Rios Luci, V. Tsikourkitoudi, Y. Deligiannakis, J. Birkenstock, S. Pokhrel, L. Madler and S. J. Soenen, *Angew. Chem., Int. Ed.*, 2020, **59**, 1828–1836.

80 L. Wang, T. Zhang, P. Li, W. Huang, J. Tang, P. Wang, J. Liu, Q. Yuan, R. Bai and B. Li, *ACS Nano*, 2015, **9**, 6532–6547.
81 Y. Toduka, T. Toyooka and Y. Ibuki, *Environ. Sci. Technol.*, 2012, **46**, 7629–7636.
82 H. Xie, M. M. Mason and J. P. Wise, *Rev. Environ. Health*, 2011, **26**, 251–268.
83 M. Farnebo, V. J. Bykov and K. G. Wiman, *Biochem. Biophys. Res. Commun.*, 2010, **396**, 85–89.
84 B. Antonsson, *Cell Tissue Res.*, 2001, **306**, 347–361.
85 J. M. Brown and B. G. Wouters, *Cancer Res.*, 1999, **59**, 1391–1399.
86 D. Jiang, P. G. Sullivan, S. L. Sensi, O. Steward and J. H. Weiss, *J. Biol. Chem.*, 2001, **276**, 47524–47529.
87 M. M. Compton, *Cancer Metastasis Rev.*, 1992, **11**, 105–119.
88 Y. Sánchez-Pérez, Y. I. Chirino, Á. R. Osornio-Vargas, R. Morales-Bárcenas, C. Gutiérrez-Ruíz, I. Vázquez-López and C. M. García-Cuellar, *Cancer Lett.*, 2009, **278**, 192–200.
89 M. J. Akhtar, M. Ahamed, S. Kumar, M. M. Khan, J. Ahmad and S. A. Alrokayan, *Int. J. Nanomed.*, 2012, **7**, 845.
90 K. Ali, Q. Saquib, B. Ahmed, M. A. Siddiqui, J. Ahmad, M. Al-Shaeri, A. A. Al-Khedhairy and J. Musarrat, *Process Biochem.*, 2020, **91**, 387–397.
91 E. Zielinska, A. Zauszkiewicz-Pawlak, M. Wojcik and I. Inkielewicz-Stepniak, *Oncotarget*, 2018, **9**, 4675.
92 S. George, S. Pokhrel, T. Xia, B. Gilbert, Z. Ji, M. Schowalter, A. Rosenauer, R. Damoiseaux, K. A. Bradley and L. Mädler, *ACS Nano*, 2010, **4**, 15–29.
93 N. Mizushima, B. Levine, A. M. Cuervo and D. J. Klionsky, *Nature*, 2008, **451**, 1069–1075.
94 M. J. Akhtar, H. A. Alhadlaq, S. Kumar, S. A. Alrokayan and M. Ahamed, *Arch. Toxicol.*, 2015, **89**, 1895–1907.
95 D. Laha, A. Pramanik, J. Maity, A. Mukherjee, P. Pramanik, A. Laskar and P. Karmakar, *Biochim. Biophys. Acta, Gen. Subj.*, 2014, **1840**, 1–9.
96 P. Vandenabeele, T. V. Berghe and N. Festjens, *Science's STKE*, 2006, **2006**, pe44.
97 J. H. Lara-González, R. Gomez-Flores, P. Tamez-Guerra, E. Monreal-Cuevas, R. Tamez-Guerra and C. Rodríguez-Padilla, *J. Adv. Med. Med. Res.*, 2013, 1308–1316.
98 P. Vandenabeele, L. Galluzzi, T. V. Berghe and G. Kroemer, *Nat. Rev. Mol. Cell Biol.*, 2010, **11**, 700–714.
99 N. B. Saleh, D. J. Milliron, N. Aich, L. E. Katz, H. M. Liljestrand and M. J. Kirisits, *Sci. Total Environ.*, 2016, **568**, 926–932.
100 E. Burello and A. P. Worth, *Nanotoxicology*, 2011, **5**, 228–235.
101 N. Odzak, D. Kistler, R. Behra and L. Sigg, *Environ. Pollut.*, 2014, **191**, 132–138.
102 M.-L. Avramescu, P. Rasmussen, M. Chénier and H. Gardner, *Environ. Sci. Pollut. Res.*, 2017, **24**, 1553–1564.
103 A. M. Studer, L. K. Limbach, L. Van Duc, F. Krumeich, E. K. Athanassiou, L. C. Gerber, H. Moch and W. J. Stark, *Toxicol. Lett.*, 2010, **197**, 169–174.
104 W. Zhang, Y. Yao, N. Sullivan and Y. Chen, *Environ. Sci. Technol.*, 2011, **45**, 4422–4428.
105 S. Elzey and V. H. Grassian, *J. Nanopart. Res.*, 2010, **12**, 1945–1958.
106 G. M. Cooper and D. Ganem, *Nat. Med.*, 1997, **3**, 1042.
107 S. Müller, J. Dennemärker and T. Reinheckel, *Biochim. Biophys. Acta, Proteins Proteomics*, 2012, **1824**, 34–43.
108 V. Sée, P. Free, Y. Cesbron, P. Nativo, U. Shaheen, D. J. Rigden, D. G. Spiller, D. G. Fernig, M. R. White and I. A. Prior, *ACS Nano*, 2009, **3**, 2461–2468.
109 X. Jiang, T. Miclăuş, L. Wang, R. Foldbjerg, D. S. Sutherland, H. Autrup, C. Chen and C. Beer, *Nanotoxicology*, 2015, **9**, 181–189.
110 W. G. Kreyling, A. M. Abdelmonem, Z. Ali, F. Alves, M. Geiser, N. Haberl, R. Hartmann, S. Hirn, D. J. De Aberasturi and K. Kantner, *Nat. Nanotechnol.*, 2015, **10**, 619.
111 J. W. Moreau, P. K. Weber, M. C. Martin, B. Gilbert, I. D. Hutcheon and J. F. Banfield, *Science*, 2007, **316**, 1600–1603.
112 J. M. Schveigkardt, A. C. Rizzi, O. E. Piro, E. E. Castellano, R. C. d. Santana, R. Calvo and C. D. Brondino, *Eur. J. Inorg. Chem.*, 2002, **2002**, 2913–2919.
113 F. Stephens, R. Vagg and P. Williams, *Acta Crystallogr., Sect. B: Struct. Crystallogr. Cryst. Chem.*, 1975, **31**, 841–845.
114 L. Antolini, *Inorg. Chem.*, 1985, **24**, 3621–3626.
115 R. Calvo, C. Steren, O. Piro, T. Rojo, F. Zuniga and E. E. Castellano, *Inorg. Chem.*, 1993, **32**, 6016–6022.
116 B. Gilbert, S. C. Fakra, T. Xia, S. Pokhrel, L. Mädler and A. E. Nel, *ACS Nano*, 2012, **6**, 4921–4930.
117 M. Chen and A. von Mikecz, *Exp. Cell Res.*, 2005, **305**, 51–62.
118 S. Linse, C. Cabaleiro-Lago, W. F. Xue, I. Lynch, S. Lindman, E. Thulin, S. E. Radford and K. A. Dawson, *Proc. Natl. Acad. Sci. U. S. A.*, 2007, **104**, 8691–8696.
119 A. A. Vertegel, R. W. Siegel and J. S. Dordick, *Langmuir*, 2004, **20**, 6800–6807.
120 S. S. Mansy and J. Cowan, *Acc. Chem. Res.*, 2004, **37**, 719–725.
121 R. H. Holm, *Acc. Chem. Res.*, 1977, **10**, 427–434.
122 D. H. Flint, J. Tuminello and M. Emptage, *J. Biol. Chem.*, 1993, **268**, 22369–22376.
123 S. S. Leal and C. M. Gomes, *Biol. Chem.*, 2005, **386**, 1295–1300.
124 P. R. Gardner, I. Raineri, L. B. Epstein and C. W. White, *J. Biol. Chem.*, 1995, **270**, 13399–13405.
125 C. Levard, E. M. Hotze, B. P. Colman, A. L. Dale, L. Truong, X. Yang, A. J. Bone, G. E. Brown Jr, R. L. Tanguay and R. T. Di Giulio, *Environ. Sci. Technol.*, 2013, **47**, 13440–13448.
126 C. m. Levard, S. Mitra, T. Yang, A. D. Jew, A. R. Badireddy, G. V. Lowry and G. E. Brown Jr, *Environ. Sci. Technol.*, 2013, **47**, 5738–5745.
127 Q. L. Feng, J. Wu, G. Chen, F. Cui, T. Kim and J. Kim, *J. Biomed. Mater. Res.*, 2000, **52**, 662–668.
128 G. V. Lowry, K. B. Gregory, S. C. Apte and J. R. Lead, *Environ. Sci. Technol.*, 2012, **46**, 6893–6899.
129 J. M. Zook, S. E. Long, D. Cleveland, C. L. A. Geronimo and R. I. MacCuspie, *Anal. Bioanal. Chem.*, 2011, **401**, 1993.
130 T. Puzyn, B. Rasulev, A. Gajewicz, X. Hu, T. P. Dasari, A. Michalkova, H.-M. Hwang, A. Toropov, D. Leszczynska and J. Leszczynski, *Nat. Nanotechnol.*, 2011, **6**, 175.

131 C. Kaweeteerawat, A. Ivask, R. Liu, H. Zhang, C. H. Chang, C. Low-Kam, H. Fischer, Z. Ji, S. Pokhrel and Y. Cohen, *Environ. Sci. Technol.*, 2015, **49**, 1105–1112.
132 Q. Mu, G. Jiang, L. Chen, H. Zhou, D. Fourches, A. Tropsha and B. Yan, *Chem. Rev.*, 2014, **114**, 7740–7781.
133 A. Verma and F. Stellacci, *Small*, 2010, **6**, 12–21.
134 F. C. Simeone and A. L. Costa, *Environ. Sci.: Nano*, 2019, **6**, 3102–3112.
135 M. V. Ganduglia-Pirovano, A. Hofmann and J. Sauer, *Surf. Sci. Rep.*, 2007, **62**, 219–270.
136 T. C. Le, H. Yin, R. Chen, Y. Chen, L. Zhao, P. S. Casey, C. Chen and D. A. Winkler, *Small*, 2016, **12**, 3568–3577.
137 R. Buonsanti and D. J. Milliron, *Chem. Mater.*, 2013, **25**, 1305–1317.
138 I. Bilecka, L. Luo, I. Djerdj, M. D. Rossell, M. Jagodic, Z. Jaglicic, Y. Masubuchi, S. Kikkawa and M. Niederberger, *J. Phys. Chem. C*, 2011, **115**, 1484–1495.
139 H. Naatz, S. Lin, R. Li, W. Jiang, Z. Ji, C. H. Chang, J. Köser, J. Thöming, T. Xia and A. E. Nel, *ACS Nano*, 2017, **11**, 501–515.
140 R. Wang, A. W. Sleight and M. Subramanian, *J. Solid State Chem.*, 1996, **125**, 224–227.
141 J. Xiao, A. Kuc, S. Pokhrel, M. Schowalter, S. Parlapalli, A. Rosenauer, T. Frauenheim, L. Mädler, L. G. Pettersson and T. Heine, *Small*, 2011, **7**, 2879–2886.
142 S. Jang and J. A. Imlay, *J. Biol. Chem.*, 2007, **282**, 929–937.
143 S. L. Chia and D. T. Leong, *Heliyon*, 2016, **2**, e00177.
144 X. Cai, A. Lee, Z. Ji, C. Huang, C. H. Chang, X. Wang, Y. P. Liao, T. Xia and R. Li, *Part. Fibre Toxicol.*, 2017, **14**, 13.
145 M. J. Osmond-McLeod, R. I. Osmond, Y. Oytam, M. J. McCall, B. Feltis, A. Mackay-Sim, S. A. Wood and A. L. Cook, *Part. Fibre Toxicol.*, 2013, **10**, 54.
146 Y. Zhang, H. Wang, H. Jiang and X. Wang, *Nanoscale*, 2012, **4**, 3530–3535.
147 H. F. Hassan, A. M. Mansour, A. M. Abo-Youssef, B. E. Elsadek and B. A. Messiha, *Clin. Exp. Pharmacol. Physiol.*, 2017, **44**, 235–243.
148 A. Kermanizadeh, K. Jantzen, M. B. Ward, J. A. Durhuus, L. Juel Rasmussen, S. Loft and P. Moller, *Nanotoxicology*, 2017, **11**, 184–200.
149 M. Benguigui, I. S. Weitz, M. Timaner, T. Kan, D. Shechter, O. Perlman, S. Sivan, Z. Raviv, H. Azhari and Y. Shaked, *Sci. Rep.*, 2019, **9**, 1–10.
150 M. A. Siddiqui, H. A. Alhadlaq, J. Ahmad, A. A. Al-Khedhairy, J. Musarrat and M. Ahamed, *PLoS One*, 2013, **8**, e69534.
151 M. Shafagh, F. Rahmani and N. Delirezh, *Iran. J. Basic Med. Sci.*, 2015, **18**, 993.
152 Y. He, Z. Du, S. Ma, Y. Liu, D. Li, H. Huang, S. Jiang, S. Cheng, W. Wu and K. Zhang, *Int. J. Nanomed.*, 2016, **11**, 1879.
153 N. E.-A. El-Naggar, M. H. Hussein and A. A. El-Sawah, *Sci. Rep.*, 2017, **7**, 1–20.
154 J. R. Nakkala, R. Mata, K. Raja, V. K. Chandra and S. R. Sadras, *Mater. Sci. Eng., C*, 2018, **91**, 372–381.
155 S. El-Sonbaty, *Cancer Nanotechnol.*, 2013, **4**, 73.
156 S. M. Dadfar, K. Roemhild, N. I. Drude, S. von Stillfried, R. Knüchel, F. Kiessling and T. Lammers, *Adv. Drug Delivery Rev.*, 2019, **138**, 302–325.
157 P. Aisen, C. Enns and M. Wessling-Resnick, *Int. J. Biochem. Cell Biol.*, 2001, **33**, 940–959.
158 T. R. Pisanic II, J. D. Blackwell, V. I. Shubayev, R. R. Fiñones and S. Jin, *Biomaterials*, 2007, **28**, 2572–2581.
159 D.-M. Huang, J.-K. Hsiao, Y.-C. Chen, L.-Y. Chien, M. Yao, Y.-K. Chen, B.-S. Ko, S.-C. Hsu, L.-A. Tai and H.-Y. Cheng, *Biomaterials*, 2009, **30**, 3645–3651.
160 S. J. Soenen, U. Himmelreich, N. Nuytten and M. De Cuyper, *Biomaterials*, 2011, **32**, 195–205.
161 H. Arami, A. Khandhar, D. Liggitt and K. M. Krishnan, *Chem. Soc. Rev.*, 2015, **44**, 8576–8607.
162 A. Van de Walle, A. P. Sangnier, A. Abou-Hassan, A. Curcio, M. Hemadi, N. Menguy, Y. Lalatonne, N. Luciani and C. Wilhelm, *Proc. Natl. Acad. Sci. U. S. A.*, 2019, **116**, 4044–4053.
163 T. Xia, Y. Zhao, T. Sager, S. George, S. Pokhrel, N. Li, D. Schoenfeld, H. Meng, S. Lin and X. Wang, *ACS Nano*, 2011, **5**, 1223–1235.
164 M. Shakir, M. Faraz, M. A. Sherwani and S. I. Al-Resayes, *J. Lumin.*, 2016, **176**, 159–167.
165 A. I. Nabeel, *Tumor Biol.*, 2020, **42**, DOI: 10.1177/1010428320909999.
166 K. Li, G. Xiao, J. J. Richardson, B. L. Tardy, H. Ejima, W. Huang, J. Guo, X. Liao and B. Shi, *Adv. Sci.*, 2019, **6**, 1801688.
167 S. Nair, A. Sasidharan, V. D. Rani, D. Menon, S. Nair, K. Manzoor and S. Raina, *J. Mater. Sci.: Mater. Med.*, 2009, **20**, 235.
168 A. Joshi, H. Naatz, K. Faber, S. Pokhrel and R. Dringen, *Neurochem. Res.*, 2020, 1–16.
169 N. Wu, C. Zhang, C. Wang, L. Song, W. Yao, A. Gedanken, X. Lin and D. Shi, *Nanomedicine*, 2018, **13**, 1303–1318.
170 X. Li, H. Xu, C. Li, G. Qiao, A. A. Farooqi, A. Gedanken, X. Liu and X. Lin, *Front. Pharmacol.*, 2019, **10**, 319.
171 R. Yuan, H. Xu, X. Liu, Y. Tian, C. Li, X. Chen, S. Su, I. Perelshtein, A. Gedanken and X. Lin, *ACS Appl. Mater. Interfaces*, 2016, **8**, 31806–31812.
172 H. Xu, R. Yuan, X. Liu, X. Li, G. Qiao, C. Li, A. Gedanken and X. Lin, *Nanomedicine*, 2019, **14**, 131–149.
173 A. Joshi, W. Rastedt, K. Faber, A. G. Schultz, F. Bulcke and R. Dringen, *Neurochem. Res.*, 2016, **41**, 3004–3019.
174 A.-K. Ostermeyer, C. Kostigen Mumuper, L. Semprini and T. Radniecki, *Environ. Sci. Technol.*, 2013, **47**, 14403–14410.
175 B. B. Manshian, J. Jimenez, U. Himmelreich and S. J. Soenen, *Adv. Healthcare Mater.*, 2017, **6**, 1601099.
176 M. I. Setyawati, X. Yuan, J. Xie and D. T. Leong, *Biomaterials*, 2014, **35**, 6707–6715.
177 M. Buttacavoli, N. N. Albanese, G. Di Cara, R. Alduina, C. Faleri, M. Gallo, G. Pizzolanti, G. Gallo, S. Feo and F. Baldi, *Oncotarget*, 2018, **9**, 9685.
178 J. Swanner, C. D. Fahrenholtz, I. Tenvooren, B. W. Bernish, J. J. Sears, A. Hooker, C. M. Furdui, E. Alli, W. Li, G. L. Donati, K. L. Cook, P. A. Vidi and R. Singh, *FASEB BioAdv.*, 2019, **1**, 639–660.

179 Z. Shaterabadi, G. Nabiyouni and M. Soleymani, *Mater. Sci. Eng., C*, 2017, **75**, 947–956.
180 M. A. Malvindi, V. De Matteis, A. Galeone, V. Brunetti, G. C. Anyfantis, A. Athanassiou, R. Cingolani and P. P. Pompa, *PLoS One*, 2014, **9**, e85835.
181 Y. Javed, L. Lartigue, P. Hugounenq, Q. L. Vuong, Y. Gossuin, R. Bazzi, C. Wilhelm, C. Ricolleau, F. Gazeau and D. Alloyeau, *Small*, 2014, **10**, 3325–3337.
182 G. Spagnuolo, V. D'Antò, C. Cosentino, G. Schmalz, H. Schweikl and S. Rengo, *Biomaterials*, 2006, **27**, 1803–1809.
183 G. Fukami, K. Hashimoto, K. Koike, N. Okamura, E. Shimizu and M. Iyo, *Brain Res.*, 2004, **1016**, 90–95.
184 H. M. El-Shorbagy, S. M. Eissa, S. Sabet and A. A. El-Ghor, *Int. J. Nanomed.*, 2019, **14**, 3911.
185 R. Tanino, Y. Amano, X. Tong, R. Sun, Y. Tsubata, M. Harada, Y. Fujita and T. Isobe, *Mol. Cancer Ther.*, 2020, **19**, 502–512.
186 E. Waidely, A.-R. O. Al-Yuobi, A. Bashammakh, M. S. El-Shahawi and R. M. Leblanc, *Analyst*, 2016, **141**, 36–44.
187 J. J. Antony, M. A. A. Sithika, T. A. Joseph, U. Suriyakalaa, A. Sankarganesh, D. Siva, S. Kalaiselvi and S. Achiraman, *Colloids Surf., B*, 2013, **108**, 185–190.
188 S. Zanganeh, G. Hutter, R. Spitler, O. Lenkov, M. Mahmoudi, A. Shaw, J. S. Pajarinen, H. Nejadnik, S. Goodman and M. Moseley, *Nat. Nanotechnol.*, 2016, **11**, 986–994.
189 C. Rodriguez-Antona and M. Ingelman-Sundberg, *Oncogene*, 2006, **25**, 1679–1691.
190 K. Nobutani, Y. Shimono, K. Mizutani, Y. Ueda, T. Suzuki, M. Kitayama, A. Minami, K. Momose, K. Miyawaki and K. Akashi, *PLoS One*, 2015, **10**, e0130032.
191 J. Liu, Y. Zhao, Q. Guo, Z. Wang, H. Wang, Y. Yang and Y. Huang, *Biomaterials*, 2012, **33**, 6155–6161.
192 A. Manke, L. Wang and Y. Rojanasakul, *BioMed Res. Int.*, 2013, **2013**, e942916.
193 T. Kurz, A. Terman, B. Gustafsson and U. T. Brunk, *Histochem. Cell Biol.*, 2008, **129**, 389–406.
194 P. Klíma, M. Laňková, F. Vandenbussche, D. Van Der Straeten and J. Petrášek, *Plant Cell Rep.*, 2018, **37**, 809–818.
195 D. J. Eide, *Biochim. Biophys. Acta, Mol. Cell Res.*, 2006, **1763**, 711–722.
196 J. H. Kaplan and E. B. Maryon, *Biophys. J.*, 2016, **110**, 7–13.
197 S. Liu, Y. Liu, B. Pan, Y. He, B. Li, D. Zhou, Y. Xiao, H. Qiu, M. G. Vijver and W. J. Peijnenburg, *Chemosphere*, 2020, **245**, 125612.